# Sequential leaching of silicified Archaean carbonates: A Rb-Sr, Sm-Nd and Pb-Pb isotopic contribution to their tectonic-thermal history (Kaapvaal Craton, South Africa)

Theofilos Toulkeridis, Norbert Clauer, I. Tonguç Uysal, Alfred Kröner

# Sequential leaching of silicified Archaean carbonates: a Rb-Sr, Sm-Nd and Pb-Pb isotopic contribution to their tectonic-thermal history (Kaapvaal Craton, South Africa)

Theofilos Toulkeridis[1], Norbert Clauer[2], I. Tonguç Uysal[3] and Alfred Kröner[4]

[1] Universidad de las Fuerzas Armadas ESPE, Sangolquí, Ecuador

[2] Institut des Sciences de la Terre et de l'Environnement de Strasbourg, Université de Strasbourg, (UdS/CNRS), 67084 Strasbourg, France

[3] Department of Geology, Faculty of Engineering, University of Istanbul-Cerrahpasa, Istanbul, Turkey

[4]Institut für Geowissenschaften, Mainz University, 55099 Mainz, Germany

## Abstract

Sequential leaching was completed by successive interactions of ultra-pure $H_2O$, HAc, HCl and $HNO_3$ with silicified/carbonated Archaean whole rocks from Barberton Greenstone belt of South Africa. The purpose of this experiment was an identification of the minerals interacting with each reagent and, therefore, a detailed succession of isotopically dated tectonic-thermal episodes recorded in these minerals. The contents of the major, trace and rare-earth elemental, together with the Sr, Nd and Pb isotopic compositions of untreated, leachate and residue triplets allowed identification and analysis of various types of carbonates and sulfates mixed with insoluble silicates. The samples yield two overall geological age milestones at 2.9 $\pm$ 0.1 and 2.1 $\pm$ 0.1 Ga, as well as varied age values, some with large uncertainties. A further event at about 1.6 $\pm$ 0.1 Ga is suggested probably in relation with the emplacement of the Bushveld complex or of further intrusive complexes of the Kaapvaal Craton.

While the basics of the different used isotopic systems can be considered to be similar, the Rb-Sr method appears to be the best suited to detail the studied rocks, especially their sensitive soluble minerals. The Sm-Nd method is less flexible because of its inherent need of widely ranging Sm/Nd ratios that depend on the mineral assemblage. In the case of the Rb-Sr

ages well constrained by isochron arrays, more similar ages were obtained by tentatively called isotrends that consist in data points slightly scattered along the arrays giving higher uncertainties, especially with the Sm-Nd method. The fact that these isotrends gave similar ages in addition to those of the isochrons comforts the historic evolution of the studied material.

These scatters most probably correspond to slight changes in the chemical characteristics of minerals leached by the successive reagents, but analytical uncertainties cannot be completely excluded, especially in the case of the $HNO_3$ leaching step. Finally, the Pb-Pb method appears to be of a more limited application, possibly because of possible metal contamination of the host rocks, either during their evolution in a region characterized by metal-rich concentrations or more recently during discrete surficial to sub-surficial alteration/weathering processes. In terms of leaching efficiency, that with $H_2O$ removed expectedly the lowest amounts of soluble components followed by $HNO_3$, the two efficient removers being dilute HAc and HCl. In turn, the obtained geochronological ages consolidate previously published ages that concentrate on post-depositional tectonic-thermal events within the Kaapvaal Craton during about 1.0 Ga. However, they also suggest some reconsideration for other ages of the literature.

**Keywords:** sequential leaching procedure; Rb-Sr, Sm-Nd and Pb-Pb isotope systematics; isochron vs. isotrend arrays; REE distribution patterns; post-depositional thermal events; Barberton Greenstone Belt

## Introduction

Carbonates represent a minor lithofacies of early Precambrian greenstone belts, but they are of interest as they are able to record tectonic-thermal steps, as well as changes of the atmospheric and oceanic environments during deposition and further recrystallization episodes (e.g., Schidlowski et al., 1975; Veizer et al., 1989; Shields and Veizer, 2002). Because of their sensitivity to multiple alteration processes, these rocks may also provide useful information about the successive post-depositional metamorphic, diagenetic and hydrothermal activities to which they were potentially subjected (e.g., Wang et al., 2018). For instance, Jahn and Cuvellier (1994) published a summary of the isotopic behavior of

carbonated Archaean rocks with useful identification aspects of successive depositional and diagenetic/metamorphic events during their evolution.

Historic information was also obtained by removing the soluble components of whole rocks in geochronological studies of Archaean carbonates with various reagents and by dating the obtained aliquots separately. In fact, since the initial Pb-Pb dating of carbonate whole rocks by Doe (1970) and later by Moorbath et al. (1987), many investigations were published to substantiate and enlarge the application of leaching techniques combined with various isotopic methods. Such applications to various sedimentary to meta-sedimentary carbonates, especially of old to very old ones that were lacking fossils of stratigraphic use, were of determining use for evaluating the potentials of new dating methods (e.g., Schwarcz and Latham, 1989; Jahn et al., 1990; Bischoff and Fitzpatrick, 1991; Luo and Ku, 1991; Erel et al., 1997; Babinski et al., 1999; Fölling et al., 2000; Melezhik et al., 2001; Bolhar et al., 2002; Kaurova et al., 2010; Bellefroid et al., 2018). These references reveal the interest of these rocks and methods for many geochronologists during decades. However, as often, such published studies did not always release unequivocal stratigraphic "ages" for various reasons, one being due to specific methodological aspects depending often on the characteristics of each isotopic method, as well as of the minerals on which they were applied. In order to increase potentially the information about the meaning of such results, especially on whole rocks that may host minerals of successive origins and/or differential evolutions, a sequential leaching procedure has been used here to evaluate further the soluble components of a few carbonates from early Archaean Barberton Greenstone Belt of South Africa. Initially, the purpose was the diversification of successively dissolved constituents by using reagents with a progressive impact on the carbonate-type minerals of the rocks. The goal was an estimation of what meant the Rb-Sr, Sm-Nd and Pb-Pb data of systems known for their variable signatures relative to successive tectonic-thermal events. In turn, a complementary goal of the study was an integrated understanding of the global evolution of these ancient rocks by a combination of various isotopic age data.

## The geological and geochronological context

Located near the southeastern edge of the Kaapvaal craton in South Africa, the Barberton Greenstone Belt consists of deformed and variably metamorphosed sedimentary and volcanic rocks of the Swaziland Supergroup (e.g., South African Committee for Stratigraphy, 1980; Fig. 1). These supra-crustal units are in structural or intrusive contact with surrounding coeval or younger granitoid plutons (Anhaeusser, 1973; Anhaeusser and Robb,

1981). The lower 8 to 10 km thick succession of this Swaziland Supergroup belongs to the ~3.5 to ~3.3 Ga old Onverwacht Group (Kröner and Todt, 1988; Armstrong et al., 1990; Lopez-Martinez et al., 1992), consisting mainly of mafic and ultramafic volcanic rocks with minor sedimentary and felsic layers (e.g., Viljoen and Viljoen, 1969; Lowe and Byerly, 2007). It is overlain, apparently conformably, by a dominantly sedimentary sequence that includes the Fig Tree and Moodies Groups.

On top of the Onverwacht Group, the predominantly sedimentary Fig Tree Group of a stratigraphic age of about 3.28 to 3.24 Ga and even to 3.22 Ga in some places (Kröner et al., 1991; Kamo and Davies, 1993) and the Moodies Group consist mostly of a 1 to 3 km thick succession of graywackes, shales, cherts, as well as of dacitic and felsic volcanics (Heubeck and Lowe, 1994; Lowe and Nocita, 1999; Eriksson and Simpson, 2000; Heubeck et al., 2013; Wabo et al., 2018). The youngest carbonate unit of this Fig Tree sequence that includes the samples studied here belongs to the Mapepe Formation (Lowe and Nocita, 1999; Drabon et al., 2019). Although virtually all Barberton rocks were affected by a low-grade metasomatic alteration that involved silicification, carbonatization and widespread crystallization of secondary sericite and chlorite, they preserved their primary structures and textures (e.g., Lowe, 1991). These reactions, especially the wide crystallization of sericite known to carry Rb are expected to impact at least the Rb-Sr system that might be the most affected by the observed metasomatic alterations.

All units of the Greenstone belt were topics of numerous geochronological (e.g., Allsopp et al., 1973; Barton et al., 1983; Armstrong et al., 1990; de Vries et al., 2006; Zeh et al., 2011; 2013; Furnes et al., 2013; Decker et al., 2015), structural (De Ronde et al., 1991; Heubeck and Lowe, 1994; Van Kranendonk et al., 2009; Grosch et al., 2011), metamorphic (Stevens and Moyen, 2007; Grosch et al., 2012; Cutts et al., 2014) and sedimentologic investigations (Eriksson et al., 1994; Lowe and Nocita, 1999; Toulkeridis et al., 1999; Westall et al., 2006; Hessler and Lowe, 2006; Hofmann and Bolhar, 2007; Heubeck, 2009; de Wit et al., 2011; Heubeck et al., 2013). The published results showed that major thermal events affected the belt after deposition of the Moodies Group at ~3.1, ~2.7, ~2.4 and ~2.1 Ga (Weis and Wasserburg, 1987; De Ronde et al, 1991; Poujol et al., 2003; Tice et al., 2004; Hofmann, 2005; Anhaeusser, 2006; Lana et al., 2011; Hofmann et al., 2013; Anhaeusser, 2014; Toulkeridis et al., 2015). However, it is needed to recall that most of these geochronological results were based on single applications of classical isotopic methods to whole rocks with complex histories and that, therefore, they may no longer be considered strictly and systematically as age milestones. More independent analytical data are certainly welcome to

consolidate the milestone ages in rocks that underwent several, sometimes discrete or even unknown events. Until now, the geochronological issue in isotopic dating of tectonic-thermal events in Archean rocks was often based on the search of already published "identical ages" rather than of specific records imprinted on specific types of rocks. A multi-method approach including three isotopic systems applied to rocks of various compositions due to specific evolutions was attempted in the herein experiment, tentatively to follow a more mineralogical than historical approach that includes successive leaching of the same rock with several impacting reagents.

The four Fig Tree carbonated rocks that were sequentially subjected here to such leaching experiments were previously part of a dating study of untreated whole rocks by the same isotopic methods (Toulkeridis et al., 1998). They belong, together with two duplicates of one of the samples, to the Mapepe Formation that is a 40-m thick sequence consisting of cherts, dolomitic carbonates and terrigenous clastic rocks of the Eastern Barite Valley (Fig. 1). This mostly carbonated rock unit contains also thin beds of jasper and translucent grey cherts with a barite horizon underneath the carbonates. The lithofacies was deposited on a well-developed shallow platform in the so-called Barite Syncline (Heinrichs and Reimer, 1977; Lowe and Nocita, 1999; Drabon et al., 2019). The selected FTG1 sample is laminated and fine-grained, consisting primarily of idiomorphic dolomite and quartz with minor Ba-rich illite that are all dispersed in a fine-silicified carbonate (Fig. 2). The three other selected samples (FTG2 to FTG4) are coarser grained and consist mostly of secondary quartz resulting from a post-depositional silicification and recrystallization of translucent dolomite and chert clasts, also resulting from a late secondary recrystallization with an extensive carbonatization. These three samples contain also ankerite, silicified dacitic ash, illite-sericite mixed layers and some chlorite clay-type minerals. All selected samples host also accessory apatite, monazite (rhabdophane), zircon and Cr-Spinel, together with minor pyrite that seems to be of primary biogenic origin. A barite-rich vein observed in sample FTG3 testifies for the occurrence of tectonic activities (Fig. 2). Similar to the FTG1 sample, the FTG1a and b samples were collected in its close vicinity as local "duplicates".

## The analytical procedure

Petrographic and stratigraphic descriptions, as well as isotopic data of the selected untreated whole rocks were already published (Toulkeridis et al., 1998). Rb-Sr, Sm-Nd and Pb-Pb dated, these rocks provide isochrons with isotopic ages of 2,632 ± 99 Ma, 2,612 ± 84 Ma and 2,743 ± 36 Ma, respectively. Significantly younger than the estimated depositional

age of ~3,260 ± 20 Ma, these ages were considered to reflect a late combined silicification and sericitization at an apparent temperature of ~200°C. Silicified after deposition, the carbonate minerals represent only up to 50 % of sample FTG1, while the other samples contain less (Table 1). In fact, several thermal events that affected the entire belt after deposition of the Fig Tree sediments (Weis and Wasserburg, 1987; De Ronde et al, 1991; Kamo and Davis, 1993; de Ronde and de Wit, 1994; Tice et al., 2004; Hofmann, 2005; Toulkeridis et al., 2010) obviously modified the mineral compositions of these rocks.

In fact, leaching techniques are applied for long, especially on clay materials of various environments with a variety of isotopic methods (e.g., Bofinger et al., 1968; Chaudhuri and Brookins, 1979; Morton and Long, 1980; Clauer, 1981; Bros et al., 1992; Clauer et al., 1993; Toulkeridis et al., 1998; Zhao et al., 1999; Clauer and Chaudhuri, 2012), while sedimentary whole rocks were leached less often, except those of Precambrian age for stratigraphic purposes. The reason for such leaching experiments is the separate analysis of the soluble and residual minerals for a differentiated evaluation of the alteration, weathering and/or re-crystallization minerals (e.g., Sahuquillo et al., 2003). It may also be recalled at this point that the real new aspect of the herein experiment is the successive leaching of the same rocks (for the initial leaching) and residues (for the following steps) by using progressively stronger reagents, which means that the further interactions did not concern the previously dissolved minerals. It might also be recalled that the prerequisite for a successful leaching experiment is in a systematic alignment of the data points of the untreated (labeled U), leachable (labeled L) and residual (labeled R) fractions of the same separates, whatever the meaning of the obtained alignment. The necessary array is clearly a matter of chemical equilibrium among the different separates and not a matter of the analyzed material. A determining advantage of such experiments is in the improved meaning of the leached concentrates by individual analyzes of their elemental contents and isotopic compositions. The relative contents allow more accurate chemical compositions for the soluble minerals mixed with the insoluble silicate minerals in the rocks, including those of economic interest identified by their trace metals. These leachable elements may result from flowing fluids that transported and concentrated specific elements during post-depositional tectonic-thermal events before incorporation into contemporaneous soluble minerals or adsorption onto insoluble minerals.

Here, the successive leaching steps were also used to evaluate the impact of the different reagents on the different types of soluble minerals, and on the residues that were expected to remain inert to the reagents. In the experiences completed here, about two grams

of powdered sediment were leached successively with distilled water ($H_2O$), 1N acetic acid (HAc), 1N hydrochloric acid (HCl) and 1N nitric acid ($HNO_3$), during 15 minutes at room temperature. De-ionized $H_2O$ and ultra-pure reagents were used at all steps of the sample preparation. While $H_2O$ and the HAc and HCl acids at a 1N concentration are considered as weak reagents with no substantial impact on any siliceous minerals (e.g., Clauer et al., 1993), $HNO_3$ is highly corrosive even at a 1N concentration with a possible impact on the silicate minerals, at least on the sensitive clay minerals. The amounts of dried powder and liquid reagent were precisely measured at each leaching step for consistent comparisons. After each step, the residues were dried gently and a given amount of each was taken and digested in a mixture of HF + $HNO_3$ + $HClO_4$ + HCl in Teflon© beakers. The major, trace and rare-earth elements (labeled REEs hereafter) were determined for both the leachates and the residues of each leaching step, together with the Sr and Nd isotopic compositions. In order to reduce as much as possible the analytical blanks, and therefore a potential analytical contamination of Pb, the whole procedure was processed with smaller amounts of sample and acids.

The elemental contents of the four whole rocks were determined on an inductively coupled plasma atomic emission spectrometer (ICP-AES of the Centre de Géochimie de la Surface of the Strasbourg University) for the majors (Al, Si, Ca, Mg, Fe, Mn and P) and one trace element (Sr), and on an inductively coupled plasma mass spectrometer (ICP-MS of the same laboratory) for two trace (Rb and Pb) and the rare-earth elements (REEs). Repeated analysis of the international standards B-EN and GL-O on a weekly basis provided an overall analytical precision of $\pm$2.5% (2$\sigma$) for the major elements, $\pm$5% for the trace elements and $\pm$10% for the REEs, on the basis of the analytical procedure by Samuel et al. (1985).

The Sr isotopic analyses were obtained on a multi-collector mass spectrometer (VG Sector of the same Strasbourg laboratory). The Sr separation was based on a chemical procedure identical to that of Schaltegger et al. (1994). The $^{87}Sr/^{86}Sr$ ratio of the NBS987 standard was of 0.710254 ± 0.000012 (2 σm external, n = 6) at the time of the study. For the isochron calculations, an average uncertainty of ± 0.000015 (2$\sigma$) was assumed for the $^{87}Sr/^{86}Sr$ ratio on the basis of the standard reproducibility, whereas the accuracy of the $^{87}Rb/^{86}Sr$ ratios was better than ± 2.5% (2$\sigma$). The $^{87}Rb/^{86}Sr$ of a few FTG1 leachates and residues were duplicated by a complete preparation and analysis for an overall control of their reproducibility. All $^{87}Sr/^{86}Sr$ ratios were corrected relative to 0.1194 for the $^{86}Sr/^{88}Sr$ ratio of the NBS987 standard.

All Sm-Nd isotopic analyses were completed on two Finnigan MAT 261 mass spectrometers (of the Max-Planck Institut für Chemie of the Mainz University Germany). The REEs were separated following the procedure of White and Patchett (1984). The $^{143}Nd/^{144}Nd$ ratios were normalized to 0.7219 for the $^{146}Nd/^{144}Nd$ ratio. During the study, the value of the $^{143}Nd/^{144}Nd$ ratio of La Jolla Nd standard was 0.511882 ± 0.000012 (2σ external, n = 10). For the isochron calculation, a routine uncertainty of ± 0.000012 (2σ) was assumed for the measured $^{143}Nd/^{144}Nd$ ratios on the basis of reproducibility of the standard. If the internal error of a single isotope analysis was larger than ± 0.000020 (2σm), the higher value was used. The $^{147}Sm/^{144}Nd$ of a few FTG1 leachates and residues were also duplicated with a complete sample preparation and analysis to control their reproducibility, while a routine uncertainty of $\pm$ 2.0% (2σ) was taken for the age calculations. All $^{143}Nd/^{144}Nd$ ratios were corrected relative to the La Jolla standard $^{143}Nd/^{144}Nd$ ratio of 0.511860.

The Pb isotope ratios were determined in a static mode on a Finnigan MAT-261 mass-spectrometer (of the Max-Planck Institut für Chemie of the Mainz University, Germany). The Pb was purified following a standard ion exchange technique (Krogh, 1973), and was measured with a mixture of phosphoric acid and Si-gel (Cameron et al., 1969) on single Re filaments. The Pb isotopes were measured individually and the Pb isotopic ratios were corrected for a mass fractionation factor of 0.1% per a.m.u., which was determined by measuring the NBS982 (Todt et al., 1996). If the internal error of an individual analysis was higher than the error defined by the 2σ value of the NBS 982, the higher value was used.

The analytical uncertainties for the alignments obtained by the three isotopic methods were calculated on the basis of Ludwig's (2003) Isoplot program and were given with the results when they appeared to be realistic and useful. The Mean Square Weight Deviates (MSWDs) that report how well more than two data points fit any correlation line are also provided when the age data of the drafted arrays were meaningful on the basis of the isochron calculations. In turn, MSWD values validate isochron lines whether the errors are of analytical or geological functions (Brooks et al., 1972). Although random variations in $^{87}Sr/^{86}Sr$ ratios induce increases of the associated MSWDs, Davidson et al. (2005) discussed how age data remain geologically meaningful even with higher MSWD values derived from variations induced by open-system mixing or contamination. Such variations can result from nicely fitting arrays but with geologically meaningless ages. In such cases, if ages are determined via varied isotopic techniques, the calculated $^{87}Sr/^{86}Sr$ ratios may provide a further insight into the petrogenetic processes resulting in the mixing of Sr with different origins.

Therefore, alignments based on somewhat scattered analytical data points from successive leaching steps, but with age values reasonably close to the ages obtained by associated isochrons, or to those obtained with other leachates and/or residues by the same or by the other isotopic methods, were not considered here as strict isochron lines but rather as trends with ages close to those of the isochrons but with uncertainties beyond the isochron reproducibility. These trends were tentatively called "isotrends" hereafter and not "errorchrons" in the sense of McIntyre et al (1966), as they are not defined on the basis of numerical calculations. In fact, they were only taken into account when their age values were within the uncertainties given by the independent associated isochrons.

## The results

Leaching with $H_2O$ provided the lowest dissolution amounts with releases between 0.12% and 0.42% of the initial whole-rock weights (Table 1). Conversely, the most efficient leaching was that with HCl that removed about 31% of the initial weight, followed by HAc that dissolved about 24%, both of the FTG1 sample. Leaching with $HNO_3$ dissolved only very small amounts of the left-over rock powders, with soluble separates of 0.5 to 1.2% of the sample weights after the already removal of the "ss" leachable material. The FGT1 sample was the most sensitive to the successive leaching steps with a global removal of 55%. The FTG2 and FTG3 samples were affected the less with about 18% of their initial weight removed, while the FTG4 sample lost slightly more of its initial weight at 21%.

*The contents of the major elements*

All leachates were analyzed for their contents in Al, Si, Ca, Mg, Fe, Mn and P that were expressed as elemental ratios (Table 2). The reagents were chosen to have each a specific impact on the selected whole rocks: the sequence started with $H_2O$ thought to dissolve preferentially the potential salts and to remove elements adsorbed on the mineral surfaces. Then HAc was chosen to remove the Mg- and Fe-carbonates and the Fe-sulfates, followed by HCl to dissolve the phosphates and the reminders of the Ca-carbonates. The last reagent was $HNO_3$ mainly to oxidize any potential organic matter, which was expected to be low in such old rocks with a possible side impact on fragile silicate components due to its high toxicity. The elemental concentrations removed by $H_2O$ were very low relative to Si taken as the immobile reference representative of the insoluble silicates. The elements removed the most by $H_2O$ were systematically Mg and Ca with ratios beyond unity relative to the

301 "conservative" Si (Table 2). The highest Ca and Mg contents with the highest Ca/Si and
302 Mg/Si ratios were obtained for the samples FTG1 and FTG3, the lowest being for sample
303 FTG2. In fact, the leachates were mostly Ca-loaded for all samples, while also enriched in Fe
304 for those of the samples FTG3 and FTG4. The contents of the HCl leachates are quite similar
305 to those of the FTG1 and FTG2 HAc leachates, while lower than those of the FTG3 and
306 FTG4 samples. The only significant contents of Ca, Mg and Fe in the $HNO_3$ leachates were
307 obtained for the FTG3 and FTG4 samples.
308 The most removed Ca, Mg and Fe record the dissolved minerals with equivalent Ca
309 and Mg amounts leached from FTG1 sample, about 2.7 times more Ca than Mg leached from
310 FTG2 sample and similarly 3.3 and 2.5 times more Ca than Mg from FTG3 and FTG4
311 samples (Fig. 2). The contents of Fe are far less: 150 to 300 times less than Ca in sample
312 FTG1, about 550 times less in samples FTG2 and FTG4 and about 1390 times less in sample
313 FTG3. By comparing the Ca/Si, Mg/Si and Fe/Si ratios of the four FGT1 $H_2O$ leachates, the
314 overall patterns are very similar with only the ratios changing (Fig. 2). In turn, the interactions
315 were quite similar for all samples with apparently equivalent mineral compositions and
316 changes only significant in the soluble amounts.
317 In sum, the four rocks are quite similar for their main mineral compositions with
318 differences in the detail of each. The Ca contents are higher than those of Mg and Fe in the
319 $H_2O$ leachates, while high Ca/Si ratios in the HAc and HCl leachates rather point to soluble
320 Ca-minerals. The high Fe/Si ratios suggest the occurrence of Fe-rich minerals, mostly in
321 sample FTG3. Leaching by $HNO_3$ appears only efficient in sample FTG3 and very attenuated
322 in sample FTG4, while the high Mg/Si ratios probably correspond to soluble Mg-minerals,
323 whereas the equivalent amounts of Mg and Ca correspond probably to dolomite that was
324 detected independently in the rocks (Fig. 3A).
325
326 *The contents and the distribution patterns of the rare-earth elements*
327 The REE concentrations of the untreated whole rocks range from 24.4 μg/g in sample
328 FTG1 to 133.3 μg/g in sample FTG2, those of the two other FTG3 and FTG4 samples being
329 of 58.2 and 67.6 μg/g, respectively (Table 4). The REE contents decrease progressively in the
330 successive leachates. With less than 0.4% of the initial rock weight, the impact of the $H_2O$
331 leaching was not evaluated further as the variations were not expected to be really
332 representative relative to the ±10% analytical uncertainty. The next leaching by HAc was also
333 almost undetectable in the total REE contents being between 1 and 0.1 μg/g lower than those
334 of the untreated rocks, which again is quite difficult to evaluate with the ±10% analytical

uncertainty (Table 3). The HCl step removed 20.4% REEs from initial content of sample FTG1, while only 2.8% from that of sample FTG2, 3.6% from that of sample FTG3 and 7.4% from that of sample FTG4. The final $HNO_3$ leaching removed 38.8% from initial REE content of sample FGT1, 10.4% from that of sample FTG2, 14.9% from that of sample FTG3 and 19.2% from that of sample FTG4.

The amounts of the heavy REEs (labeled hereafter HREEs) increase in the residues of the HAc leaching, while the $HNO_3$ leachates are enriched in HREEs with a Gd/Yb ratio up to three times that of the corresponding residues. The fact that the HAc leaching did not induce any decrease of the total amounts of REEs in any of the four samples implies that the dissolved minerals were notably depleted in REEs. The following HCl leaching removed 20.8% REEs from FTG1 sample, as well as 3.4%, 2.7% and 7.4% from FTG2 to FGT4 samples, sucessively. The final $HNO_3$ leaching removed 18.7% REEs of sample FTG1, 7.5% of sample FTG2, 9.5% of sample FTG3 and 11.8% of sample FTG4.

It might be quickly recalled that REE distribution patterns of geological materials are often compared to a standard/reference material. Here, the patterns of the successive leachates were compared to that of standard chondrites (Evensen et al., 1978), which is a usual choice for Precambrian sedimentary materials because both the analyzed rocks and the standard material are often of similar types and origins. In fact, younger sedimentary rocks are more often compared to either the North-American Shale Composite (NASC; Gromet et al. 1984) or the Post-Archaean Australian Shales (PAAS; Taylor and McLennan, 1985). There is no fundamental difference about comparing the REE contents of sediments and metasediments with any of these three references, except that it is easier to visualize variations of a flat pattern such as those relative to the PAAS and/or NASC and not relative to an inclined one like that of the chondrites. The REE contents and distribution patterns of Fig Tree shales were already analyzed by McLennan et al. (1983) who found that they are characterized by variable patterns with high La/Yb ratios of 5.5 ± 1, which corresponds to an inclined pattern towards less HREEs. Relative to the chondrite reference, all untreated whole rocks and all corresponding residues yield here similar inclined decreasing REE distribution patterns with a positive Eu anomaly and a smooth incurved end for the heaviest REEs (Fig. 4A). In the detail, the patterns of the FTG2 and FTG4 samples are similar, whereas that of sample FTG1 is more widely scattered with a positive Tm anomaly and that of sample FTG3 yields a negative Tm anomaly (Fig. 4B). These different Tm contents refer, most probably, to analytical aspects due to very small contents at the detection limit of the used equipment.

When compared to the PAAS patterns, those of the untreated samples, the residues and the leachates are quite similar (Fig. 4B). In the detail, only the amounts are changing with patterns showing a very constrained light REE (labeled LREE hereafter) distribution until Sm, then a significant positive Eu anomaly with an intensity depending on the type of used reagent. From Eu to Lu, the HREEs give again a flat pattern but with a more dispersed distribution than that of the LREEs. In fact, only the $HNO_3$ leachates yield very low contents with, however, a pattern relatively similar to the solid and liquid aliquots. In the detail, the patterns of the leachates show significantly lower contents from La to Sm and from Gd to Lu relative to those of the untreated whole rocks and of their residues. Those of the leachates are also less inclined towards the HREEs, while more scattered relative to the chondrite reference (Fig. 4C). Only those of the FTG1 sample yield a pronounced positive Eu anomaly, as for the other residues. This Eu anomaly is changing in the different leachates of the same FTG1 sample: highest in that by $HNO_3$ leaching and lowest in that by HCl leaching. The $HNO_3$ leachates yield systematically the lowest REE contents, with the most positive Eu anomaly for the pattern of sample FTG1. Highest in the HCl leachates, this anomaly relates to the systematic occurrence of Ca-carbonates in the four samples, except in the $HNO_3$ leachate where no Ca-carbonate remains and for which it cannot be excluded that it suggests a silicate alteration by the reagent.

In summary, the REE distribution patterns relative to either the chondrites or the PAAS are not intrinsically determining in the delineation of the mineral compositions and the historic evolution of their host rocks. However, they are helpful in decrypting the intensity of the impacting events. The patterns relative to the PAAS are quite similar from lightest to the heaviest REE except the systematic variation in the Eu anomaly (Fig. 4). Close to that of the untreated sample, the highest Eu anomalies are those of the residues after the $H_2O$ leaching. The next highest Eu anomalies are, then, those of the HAc, HCl and $HNO_3$ residues. In the case of the leachates, the highest Eu anomaly is that of the HAc leachate, followed by those of the HCl and $HNO_3$ leachates.

*The Rb-Sr isotopic data*

The $^{87}Sr/^{86}Sr$ ratios of the residues increase systematically after each leaching step, while those of the leachates become less radiogenic after the successive $H_2O$, HAc and HCl leaching steps (Table 5) and are widely dispersed for the $HNO_3$ residues. The reagents alter differentially the constituting minerals of the initial rocks, as the variations do not result from analytical problems. Indeed, six analytical differences amongst two independent analyses of

the same $^{87}Rb/^{86}Sr$ ratio were below $\pm$3.1% (2σ); only the reproducibility of the $HNO_3$ experiments was higher at $\pm$3.7% and $\pm$9.0% (2σ; Table 5). Also, the plot of the untreated, leachate and residue aliquots along single arrays in isochron diagrams guaranty well-done experiments without any loss of any of the components from the separates (Fig. 5), the next step depending then on how the obtained arrays can be identified as isochrons with meaningful ages.

Due to the extremely limited amounts of elements removed by the $H_2O$ leaching, the corresponding residues can be assimilated to the untreated samples, with the HAc leachate and residue data points fitting the same array, for instance in the case of the FTG1 and FTG2 samples. The data points of the HCl leachate and residue of sample FTG2 plot slightly above and below the array drawn through the HAc leachate and residue data points (Fig 5). On the other hand, the data points of the $HNO_3$ leachate and residue of sample FTG1 are dispersed away from the two arrays. In the case of sample FTG3, the lower array with the lowest slope includes the data points of the HAc leachate and residue, while the upper line integrates the data points of the two HCl leachates with a nearby data point of the $HNO_3$ residue. Furthermore, the data point of the $H_2O$ residue plots just below the lower array, together with that of the untreated rock. The results of sample FTG4 are slightly scattered with a similar $^{87}Sr/^{86}Sr$ ratio for the HAc, HCl and $HNO_3$ leachates, together with an unexpected high $^{87}Rb/^{86}Sr$ ratio for the $HNO_3$ leachate. The HCl residue yields very high ratios, while the data point of the untreated rock (in red) plots slightly below the line joining the data points of the HCl leachate and residue.

The ages and the initial $^{87}Sr/^{86}Sr$ ratios were calculated for the arrays of the four samples (Fig. 5). The lower of the two lines obtained for sample FTG1 are based on the HAc leachate and the data points of the untreated and $H_2O$ leached whole rock. It yields an age value of 2,182 $\pm$ 47 Ma (MSWD = 0.95) for an initial $^{87}Sr/^{86}Sr$ ratio of 0.7062 $\pm$ 0.0002. The array above consists of one HAc leachate, one HCl leachate and one $HNO_3$ residue that appears to be an heterogeneous assemblage as the HNO3 leachate is clearly away from the other data points, especially from other leachates with an abnormal high $^{87}Rb/^{86}Sr$ ratio.

The results of FTG2 sample raise an interesting duality between the data points of the HCl leachate and residue and a HNO3 residuethat give a high age value of 2,971 $\pm$ 64 Ma (MSWD = 0.02) and an initial $^{87}Sr/^{86}Sr$ ratio of 0.7093 $\pm$ 0.0003. The two data points of the HAc leaching give a second array with the untreated whole rock (in red) and a $H_2O$ residue with a significantly lower age value of 2,222 $\pm$ 41 Ma (MSWD = 2.2) that is within the age range of the FTG1 data. The data points of the untreated whole rock of sample FTG3 with the

$H_2O$ residue and the HAc leachate give a further isochron array with a close age of 2,461 ± 51 Ma (MSWD = 1.5) and an initial $^{87}Sr/^{86}Sr$ ratio of 0.7143 ± 0.0001. To be mentioned also is the very high initial $^{87}Sr/^{86}Sr$ ratio of 0.7243 ± 0.0003, far above the 0.7062 ± 0.0002 obtained for the array fitting the HCl data of the FTG1 sample and giving a similar age. The difference between the data of the HAc and the HCl leachates is confirmed by the results of the same FTG3 and FTG4 leachates. The arrays through the HCl data points also provide systematically the highest age values in both cases, being even unrealistic beyond 3.8 Ga. The initial $^{87}Sr/^{86}Sr$ ratios of the HAc and HCl arrays are also significantly different; that of the HCl lines range narrowly from about 0.706 to 0.709, while that of and with the HAc leachates varies widely from about 0.706 to 0.724. The $HNO_3$ leachate of FTG3 sample yields the almost lowest $^{87}Sr/^{86}Sr$ ratio for the almost highest $^{87}Rb/^{86}Sr$ ratio.

In summary, leaching with dilute HCl and HAc does not provide similar results for both the leachates and the residues. Obviously, the two experiments did not remove the same soluble minerals, which was expected by the sequential mode unless they dissolved identical minerals but of different chemical compositions and necessarily of different generations. The HCl leaching gives arrays that yield systematically steeper slopes and, consequently, higher age values than those of the corresponding HAc leaching. Some of these age values are even unrealistic, beyond the probable deposition age of the Fig Tree sediments, which favors an identification of mixing lines and not isochrons. In this case the HCl leaching probably affected at least the retention capabilities of other soluble minerals than the plain carbonates. A further remark is for the $HNO_3$ leaching that gives either similar or very different $^{87}Sr/^{86}Sr$ ratios for the leachates and the residues, depending on the leached samples. This strongly suggests that the reagent dissolved minerals of a composition similar or even identical to that of the insoluble residual minerals, unless altering slightly some fragile silicate minerals with a few release of Rb and Sr. On the basis of the strict analytical results, the HAc leaching provided several times age data of about 2.2 and 2.9 Ga as solid age references, with also a collective age of 2,799 ± 42 Ma for all the residues.

*The Sm-Nd isotopic data*

The trends of the leachate and residue data points obtained by the Sm-Nd system are similar to those of the Rb-Sr method (Table 5; Fig. 6), the main difference being in the respective locations of the data points in an isochron diagram. In contrast to those of the Rb-Sr system, the leachates yield higher $^{143}Nd/^{144}Nd$ ratios than their corresponding residues and, therefore, plot farther away from the array origins than the residues (e.g., Bros et al., 1992).

There is another difference along with the Rb-Sr method, namely the analytical precision of the Sm-Nd isochron ages that strongly depends on the $^{143}Nd/^{144}Nd$ spread of the separates due to the limited disintegration of the $^{147}Sm$. Here, the quite narrow spread in the $^{147}Sm/^{144}Nd$ ratio from 0.09 to 0.22 with large errors of the age data are then, together with small MSWDs, indicative of satisfying analytical conditions. Also to be mentioned is the analytical uncertainty between three analyses of the same $^{i47}Sm/^{144}Nd$ found to be below $\pm$2.9% (2σ) except for the HCl and HNO3 experiments which data range at $\pm$4.2% and $\pm$8.3%, respectively (2σ; Table 5). It has then been decided to provide hereunder all the analytical errors for completeness, not considering all of them in the comparisons with the other isotopic results and in the discussion about the age meaning (Fig. 6).

The data points of five FTG1 residues, the three HAc residues and the HAc and HCl residues fit an array with an age value of 2,002 $\pm$ 140 Ma (MSWD = 2.1) and an initial $^{143}Nd/^{144}Nd$ ratio of 0.5095 $\pm$ 0.0002 (2σ). An alignment through the data points of the FGT2 HAc and HCl leachates and of the $H_2O$, HAc, HCl and $HNO_3$ residues yields an age value of 2,831 $\pm$ 560 Ma (MSWD = 4.3) with a large uncertainty and an initial $^{143}Nd/^{144}Nd$ ratio at 0.5086 $\pm$ 0.0005 (2σ). The sample FTG3 yields the same display with the same leachate and residues data points for another close age of 2,930 $\pm$ 290 Ma (MSWD = 0.03), a large uncertainty and an identical initial $^{143}Nd/^{144}Nd$ ratio of 0.5086 $\pm$ 0.0003 (2σ). The two HCl points fit a slightly steeper array with an age value of 3,343 $\pm$ 440 Ma and an initial $^{143}Nd/^{144}Nd$ ratio of 0.5082 $\pm$ 0.0004 (2σ). Finally, the two HAc and the two HCl data points, together with those of the untreated whole-rock and the $HNO_3$ residue of sample FGT4 fit an array with an age value of 3,922 $\pm$ 490 Ma (MSWD = 0.25) for an initial $^{143}Nd/^{144}Nd$ ratio of 0.5078 $\pm$ 0.0004 (2σ), which is unrealistic because of the theoretical deposition age of the sedimentary sequence and because of its large uncertainty. The complementary HCl line through the leachate and residue data points yields a far younger age data of 1,444 $\pm$ 180 Ma for an initial $^{143}Nd/^{144}Nd$ ratio of 0.5083 $\pm$ 0.0003. This is the only significantly younger age value obtained here, but as the array was drawn only through two data points it is of weak constrain.

In summary, leaching with HCl and HAc does not provide similar Sm-Nd ages as was already the case for the Rb-Sr method, which confirms indirectly that the reason is in the samples, not in the methods. Also, the Sm-Nd age values of sample FTG4 give unrealistically high and low values, while the $HNO_3$ leaching provides unexpectedly similar $^{147}Sm/^{144}Nd$

ratios for the leachates and the residues, as was also the case for the Rb-Sr method. About the strict analytical data, one average age value concentrates at 2.9 Ga.

*The Pb-Pb isotopic data*

The $H_2O$ residues of the four FTG samples were analyzed by the Pb-Pb method, together with the HAc, HCl and $HNO_3$ leachates and the HAc and $HNO_3$ residues of the FGT1 and FGT4 samples (Table 6). The $^{206}Pb/^{204}Pb$ ratio decreases for the successive leachates of sample FTG3, while the $HNO_3$ leachates of the other three samples became more radiogenic. In an isochron diagram, the data points range along trends, however not precisely enough to allow age calculations with reasonable uncertainties. In fact, only four data points of sample FTG4, three leachates and one residue, plot along an array that yields an age value of 2,032 $\pm$ 48 Ma (MSWD = 2.5; Fig. 7A). In fact, the Pb-isotopic data of the leachates and residues from the four samples scatter around two major trends (Fig. 7B): an upper one includes only the data points of sample FTG1 and a steeper one with the data points of the other samples. These Pb-isotopic data outline more or less parallel arrays that were tentatively identified as "isotrends" with average ages and acceptable uncertainties, like for the two other methods, rather than "isochrons" with more constrained ages and uncertainties. The differences between well-defined isochrons and less-defined isotrends may then be due to: (1) the fact that soluble Pb yields variable isotopic compositions due to various origins and/or mineral combinations, or to recent altering contamination(s), (2) a potential contamination during the handling and preparation of the samples that can also not be excluded, and (3) a variable natural Pb-isotope composition, especially in the leachates, suggesting a variable alteration of metal-rich rocks subjected to a natural metal alteration. However, some of the Pb-Pb ages, such as that at 2,032 $\pm$ 48 Ma, set reliable milestones and, consequently, are not supportive of a continuous natural contamination by metallic ore concentrates.

## Discussion

The collective Rb-Sr data of the $H_2O$ residues organize into an alignment that can be assimilated to an isochron with an age of 2,799 ± 42 Ma that fits well with the 2,632 ± 99 Ma for the previously published isochron of the untreated whole rocks (Toulkeridis et al., 1998). The very gentle action of $H_2O$ explains this proximity as a surface cleaning of the constitutive minerals. Despite large analytical errors due to the limited spread of the Sm/Nd ratio, the corresponding ages for the HAc and HCl residues are close to that of the untreated rocks,

535 while the results of the $HNO_3$ leaching are unexpectedly scattered and therefore questionable.
536 In fact, the Sm-Nd method provides the above identified isotrends rather than isochrons
537 because of the slight mentioned spread of the Sm/Nd ratio, but further isotrends with
538 significant errors can also be identified. The $H_2O$ leachates and residues of the FTG2 to FTG4
539 samples give Pb-Pb isochrons, while those of sample FTG1 rather fit the just defined
540 isotrends. These less precise alignments confirm that the Pb-Pb data suggest different
541 elemental sources or generations for soluble Pb-carrying minerals, unless an unexpected
542 analytical aspect needs consideration. The main question becomes then the identification of
543 the different compositions of the soluble leachates and of the residues after the interaction
544 with each reagent.

545 As already mentioned, published stratigraphic ages are often based on single leaching
546 experiments with single-method ages, by combining the data of multiple untreated rocks or
547 minerals, sometimes with the corresponding leachates and residues. Indeed, the assumption
548 for such attempts was, admittedly, the age value of the data identifying a supposed event
549 (deposition, diagenesis or metamorphism) responsible for the isotopic homogenization of the
550 used isotopic system. Designed as a multi-control of leachates and residues subjected to a
551 long and complex history, therefore with varied mineral compositions, the method consists
552 here to identify the traces and the epochs of the successive impacting events on the basis of of
553 distinguishing various dissolved minerals and residues. A preliminary comment is about the
554 obtained isotopic data that give, whatever the isotopic system, less precise alignments than
555 usual isochrons that were tentatively replaced by the above defined "isotrends". The analytical
556 dispersion of these isotrends seems to be due to limited but sensitive variations in the
557 chemical and also in the isotopic compositions of the constitutive minerals with various
558 reactions depending on the used reagents (Fig. 8). It may also be mentioned that minor
559 analytical problems can never be excluded completely along the sample preparation and
560 spectrometric analysis, even if most variations obtained here seem to be due to natural and not
561 analytical aspects.

562

563 *The isotopic "ages" of the leachates*

564 The graphical distribution of the data points from untreated whole rocks provides an
565 initial alignment with noticeable differences in the Sr contents of the samples. Sample FTG1
566 yields clearly an overwhelming content of Sr relative to an $^{87}Rb/^{86}Sr$ ratio below 0.5. On the
567 other hand, the FTG3 and FTG4 samples consist of more insoluble minerals giving an
568 $^{87}Rb/^{86}Sr$ ratio above 3, which is close to that of sample FTG2 (Fig. 9C). These differences

result from varied lithofacies of the samples, confirmed in turn by the Ca/Si ratio of the HCl leachates that is to say by the ratio of the soluble relative to the insoluble minerals. This Ca/Si ratio is of 50.4, 14.5, 121 and 14.5 for the four FTG1 to FTG4 samples, respectively. The highest ratio of 121 for sample FTG3 with, by far, the highest Fe/Si ratio corroborates the occurrence of a Fe-rich soluble phase.

The comparison of the Rb-Sr results from leachates shows that those of sample FTG1 by HAc plot very narrowly (Fig. 9A and B). This plot confirms that the leaching experiments were completed correctly within analytical uncertainty, and that the analytical dispersion of the leachates from the other samples are due to natural mineralogical heterogeneities of the rocks. Dispersed relatively to those of the HAc leachates, the equivalent HCl and $HNO_3$ data result from dissolution of minerals that were necessarily heterogeneous in their Sr isotopic composition. Consequently, the array through the data points of the untreated whole rocks is not a true isochron but rather a mixing line because of that lack of Sr isotopic homogeneity. Also to be noticed are the identical trends for the HCl and HAc leachates of the FTG1 to FTG3 samples (Fig. 5).

On the basis of the Rb-Sr results, it is clear that the untreated rocks contain soluble minerals that reacted variably depending on the used reagent. Sample FTG1 reacts to HAc with leachates loaded in Ca and consists therefore mostly of Ca carbonates, while the HCl leachates are loaded in Fe and therefore of probable Fe-enriched carbonates and/or sulfates. The fact that the HCl leachates give arrays with steeper slopes suggests that the Fe-rich minerals may be older than the other minerals, or that they were subjected to a lower degree of remobilization/recrystallization than the Ca-rich counterparts. On the other hand, the age values of the HCl separates may yield age values older than the probable deposition age of the Fig Tree sediments, suggesting in turn that some of these carbonates could even contain relicts of detrital origin, but which is not realistic for soluble minerals that are expectedly sensitive to any post-depositional thermal alteration. It could also be that leaching removed also Rb off the corresponding residues that decreased their Rb/Sr ratio and consequently increased their corresponding age values. The conclusion about the $HNO_3$ leaching impact is also not immediate, as it provides similar $^{87}Sr/^{86}Sr$ ratios for the leachates and the residues with unexpected high $^{87}Rb/^{86}Sr$ ratios for the leachate of samples FTG1 and FTG4, together with a high $^{87}Sr/^{86}Sr$ ratio for the latter. The identical $^{87}Sr/^{86}Sr$ ratios for both the leachate and the residue also point toward a congruent dissolution of residual material with $^{87}Sr/^{86}Sr$ ratios similar to those of the leachates.

602 The Sm-Nd data points of the HAc and HCl leachates plot also on separate
603 alignments, as do those of the $HNO_3$ leachates (Fig. 10). All these lines yield increasing
604 positive slopes with increasing Sm/Nd ratios. The "curvy" organization of the four lines
605 through the leachate points has already been identified as an analytical prove for
606 heterogeneous materials: the $HNO_3$ leachates build the lower branch of the composite curve,
607 while the HAc line represents the intermediate trend of the curve and the HCl line the upper
608 section. None of these arrays yields meaningful stratigraphic ages, as the HCl and HAc
609 leachates of sample FTG3 plot even outside the lines through the leachate points. In fact, they
610 plot quite narrowly but on two lines with data points of residues, as will be discussed in a
611 further section. The age data calculated for sample FTG4 give unrealistically high values
612 beyond the admitted deposition time of the sediments, while the $HNO_3$ leaching gives,
613 surprisingly, similar $^{147}Nd/^{144}Nd$ ratios for the leachates and the residues. The Pb-Pb results
614 of the FTG2, FTG3 and FTG4 leachates can be organized into three sub-parallel isotrends
615 consisting of heterogeneous separates. The age values are of 2,800 $\pm$ 260 Ma (MSWD = 8.2),
616 2,850 $\pm$ 760 Ma (MSWD = 4.2) and 2,749 $\pm$ 490 Ma (MSWD = 12.0) for the three arrays
617 consisting each of four data points. It is very tempting to suggest that these data focus on a
618 unique tectonic-thermal event that occurred at about 2.8 $\pm$ 0.5 Ga.
619 In summary, the overall Rb-Sr, Sm-Nd and Pb-Pb results suggest that two important
620 events occurred in this region of the Barberton Greenstone Belt at 2.9 $\pm$ 0.1 and 2.1 $\pm$ 0.1 Ga,
621 as well as one or several less intruding episodes between 1.6 and 2.0 Ga (Table 7). These
622 milestones are also confirmed by several isotrends giving similar age values but with large
623 uncertainties.
624
625 *The isotopic "ages" of the residues*
626 Taken together, the Rb-Sr data of the residues show an incurved distribution with a
627 changing angle for the upper HAc data points (Fig. 11A). Such a display characterizes
628 heterogeneous materials, either as whole rocks or as size fractions (e.g., Clauer et al., 2020).
629 When plotted in the same diagram, all data points of the residues organize into distinct
630 patterns resulting from either "gentle" $H_2O$ and HAc leaching on the lower linear branch, or
631 from $HNO_3$ leaching on a sub-parallel linear trend above the previous one, whereas that of the
632 HCl reagent gives the upper display (Fig. 10A). The consequence is that these results,
633 especially those of the HCl leaching, yield age values that are geologically meaningless. Once
634 again, sample FTG3 contains a heterogeneous component clearly reactive to the HCl
635 leaching.

636 The Rb-Sr age calculations of the different residues give several arrays (Fig. 11A).
637 That based on three residues of the $HNO_3$ leaching yields a high isotrend age value of about
638 3,754 $\pm$ 710 Ma (MSWD = 26) with a high analytical uncertainty. On the lower side, the data
639 points of five $H_2O$ residues fit a line with an age of 2,799 $\pm$ 42 Ma (MSWD = 0.04) and an
640 initial $^{87}Sr/^{86}Sr$ ratio of 0.7009 $\pm$ 0.0007. This value may, again, be considered as meaningful
641 with an acceptable initial Sr ratio for such old sediments. The data points of more $H_2O$
642 residues fit a sub-parallel isotrend with a similar age of 2,764 $\pm$ 240 Ma.
643 The Sm-Nd data of all residues were also combined in a single isochron diagram (Fig.
644 10B). The $HNO_3$ residues of sample FTG1 yield the flattest trend, while those of the three
645 other samples fit an independent line, also with a very low slope. By contrast, most data
646 points of the $H_2O$ and HAc residues plot on an array with an age of about 2.9 Ga and an initial
647 $^{143}Nd/^{144}Nd$ ratio of about 0.5086, the large errors suggesting again an isotrend. The data
648 points of the FTG3 and FTG4 residues plot narrowly, also on an isotrend with a slope sub-
649 parallel to the previous one.
650 The Pb-Pb data of the residues plot on an array with a steep slope (Fig. 7), but which
651 data points are widely scattered, and therefore with a high uncertainty. In fact, these results do
652 not add much to the already available age values obtained by the Rb-Sr and Sm-Nd methods.
653 However, the Pb-Pb age between 2.75 and 2.85 Ga is confirmed by the already published Rb-
654 Sr and Sm-Nd results of the residues.
655
656 *Meaning of the leachate-residue "ages"*
657 The data of the sequential leaching support the hypothesis that the whole rocks studied
658 here contain various soluble minerals that react variably depending on the used reagent.
659 About the calculated age values, the alignment of the HAc leachates and residues of FTG1
660 sample provides a Rb-Sr isochron representative of the Ca-carbonate at 2,182 $\pm$ 47 Ma, also
661 obtained for sample FTG2. On the basis of given mineral contents from the rock suite, the
662 purpose becomes a stepwise separation of soluble phases in order to quantify their
663 compositions and, therefore, sort out their specific histories. The determination of the REE
664 contents was expected to support the identification of individually dissolved minerals. In turn,
665 it cannot be excluded that beyond the dissolution of the soluble minerals and surface cleaning
666 of the insoluble minerals, some of these silicate minerals were also altered slightly especially
667 by the $HNO_3$ leaching. It may explain the high or at least unusual radiogenic signatures for
668 some of the arrays (e.g., Fig. 5 and 6) for which the obtained age values are also older than the
669 depositional age. It cannot, furthermore, be ignored that he obtained results suggest also

potential detrital provenances. Given the results, the Archaean rocks could have also been subjected during their long and disrupted evolution to some contamination/pollution, not by the present-day atmosphere but during the tectonic-thermal episodes that might have induced some scattering by long-distance migrations of exotic fluids. This could especially have been the case for the Pb-Pb method highly dependent on a strict closed behavior of the metal carriers.

In summary, the combined application of the Rb-Sr, Sm-Nd and Pb-Pb dating methods on various types of leachates and associated residues of a few samples enabled to contribute to the reality of isotopic ages at 2.9 $\pm$ 0.1 and 2.1 $\pm$ 0.1 Ga for the studied Fig Tree metasediments (Table 7). On the basis of the data of the classical untreated whole-rock technique (Toulkeridis et al. 1998), these ages probably resulted from large-scale fluid movements generated by successive tectonic-thermal activities already described elsewhere. The slightly older 2.4-Ga age obtained by $^{40}Ar/^{39}Ar$ ages of altered barite from Barberton Greenstone Belt (De Ronde et al., 1991) was only obtained here by an isotrend and could be part of either the start or the end of the two longer and better constrained tectonic-thermal episodes around. Indeed, the 2.0 Ga age obtained more or less precisely by the Sm-Nd method on sample FTG1 is correlative with the emplacement of the Bushveld complex and other intrusive complexes in the Kaapvaal Craton. It was obtained previously by $^{40}Ar/^{39}Ar$ dating of sedimentary rocks (De Ronde et al., 1991) and biotites of surrounding granodiorites (Layer et al., 1992), as well as by Rb-Sr dating of cherts (Weis and Wasserburg, 1987). It propagated most probably at a quite low closing temperature of ~130°C with some quartz recrystallization. Also not formally confirmed by a Rb-Sr age of sample FTG1, the younger age at ~1.7 Ga was unknown as a widespread event in the Kaapvaal Craton, but was reported previously by $^{40}Ar/^{39}Ar$ dating of highly altered basaltic pillows (Layer et al., 1992).

*The isotopic results of the variously leached rocks*

Identical ages obtained by various isotopic methods after leaching different types of whole rocks appear appropriate to distinguish evolution steps of especially old rocks that underwent multiple tectonic-thermal impacts of varied intensities. The geologically meaningful ages at 2.9 $\pm$ 0.1 and 2.1 $\pm$ 0.1 Ga obtained here on various carbonated rocks supports the reality of these two historic milestones in the early evolution of the Archaean carbonate-rich Fig Tree samples. Also, the isotopic methods applied at different leachates and residues provided also some isotrends that comfort the isochron ages with larger uncertainties. Therefore, leachates obtained by different reagents that give reasonably close ages even if less

constrained confirm that: (1) the use of reagents of variable intensity combined with different isotopic methods is appropriate; (2) isotrends do not necessarily result from analytical problems; and (3) the ages obtained by the isotrends help constrain age data given by identified isochrons. As a further comment, it looks like the Pb-Pb method is the less adequate of the used isotopic methods for such attempts as the data scatters could also be contaminated by external facts due to the natural behavior of Pb isotopes. In turn, it cannot be excluded that the analytical Pb-Pb dispersion was also impacted by the regional metalliferous context of the samples and result from labile behavior of Pb during a multi-composite evolution and/or possibly to a recent to present-day pollution that would need to be identified.

The initial isotopic ratios of the isochrons and the isotrends from leachates may also provide information about the chemistry of the interacting fluids. The initial $^{87}Sr/^{86}Sr$ ratios are often dispersed between 0.706 and 0.720, including the initials of the arrays giving unrealistic old age data. It looks like the authigenic soluble minerals of the successive tectonic-thermal events yielded variable Sr isotopic signatures that relate to the signatures of the potential interacting fluids. For instance, the arrays of about 2.8-2.9 Ga were obtained with initial $^{87}Sr/^{86}Sr$ ratios at 0.7093 $\pm$ 0.0003 ($\pm 2\sigma$), 0.7143 $\pm$ 0.0001 and 0.7200 $\pm$ 0.0004. Conversely, the initial $^{143}Nd/^{144}Nd$ ratios of the alignments are consistently narrower for each isochron or isotrend. Those of the lines with slopes about 2.8-2.9 Ga are at 0.5086 $\pm$ 0.0005 ($\pm 2\sigma$) and 0.5086 $\pm$ 0.0003, and that of the line at about 2.1 Ga is of 0.5095 $\pm$ 0.0002 ($\pm 2$). The limited number of Pb-isotopic data does not allow such a comparison of the initial ratios of the Pb-Pb arrays.

In summary, the initial ratios of the isochrons and of the isotrends provide basics for the Rb-Sr and the Sm-Nd methods. The Sr isotopic identity of the Rb-Sr method is quite dispersed, whereas the Nd identity of the Sm-Nd method is much more concentrated, therefore focusing on different compositions, origins and possibly temperatures for the associated fluids. The Rb-Sr isotopic "world" appears much more heterogeneous than that of the comparative Sm-Nd system. However, it is actually difficult to relate these types of results to precise events and processes that are as old as 2.8 Ga.

*The evolution of the Kaapvaal Craton based on the data of the leachates*

The overall similar REE distribution patterns of the residues suggest that the silicates yield narrowly similar mineral compositions, except for a more diversified assemblage for sample FTG1, for which the successive residues of the same FTG1 sample yield, however, very close patterns (Fig. 4B). Furthermore, the systematic positive Eu anomaly detected in the

738 leachates and the residues of the samples analyzed here excludes, in turn, its traditional
739 relation with the occurrence of detrital plagioclase feldspars, but operates rather as a function
740 of temperature and oxygen fugacity (Weill and Drake, 1973). The reason for the abnormal
741 occurrence of Eu resulted then from: (1) tectonic-thermal episodes that altered feldspars of the
742 meta-sediments, or (2) released REEs disseminated in various types of minerals including
743 soluble ones. In fact, MacRae et al. (1992) reported positive Eu anomalies in diagenetically
744 impacted sediments with Eu considered to precipitate in the $3^+$ state when the environment
745 was of oxidation potential. Just before, Bau (1991) predicted that oxygen fugacity increasing
746 with the temperature, the fluid-rock interactions under mild acidic conditions favor a positive
747 anomaly. Nakada et al. (2019) showed also that positive Eu anomalies can occur when water
748 interacted with the rocks at hydrothermal conditions below 100°C. Along the study of this
749 positive Eu anomaly in Precambrian sediments, Banded Iron Formations older than 2.5 Ga
750 from various sites of North America, Finland and Australia were found to yield positive Eu
751 anomalies, while younger ones did not (Danielson et al., 1992; Bolhar et al., 2004). The
752 former authors also stated that the anomaly seems to be dominantly driven by hydrothermal
753 conditions with solution temperatures above 175°C. Kato et al. (1996) reported also positive
754 Eu anomalies in Banded Iron Formations of India and suggested that they were of
755 hydrothermal origin. In summary, the positive Eu anomaly seems to have been driven by low-
756 temperature oxidizing hydrothermal conditions in Banded Iron Formation older than 2.5 Ga.
757 The widely tectonic-thermal events described in the craton and dated isotopically appear,
758 therefore, as favorable conditions to the occurrence of the Eu anomaly detected in the soluble
759 and insoluble mineral phases studies here.
760 The large number of geochronological studies on South-African Archaean meta-
761 sediments has shown that the whole Barberton Greenstone Belt was affected by several
762 tectonic-thermal events during its complex evolution. Based on the literature, five events were
763 identified at ~3.45, 3.25, 3.1, 2.7, and 2.1–2.0 Ga (e.g., Weis and Wasserburg, 1987; Lopez-
764 Martinez et al., 1992; Kamo and Davis, 1994; Lécuyer et al., 1994). The ~2.7-Ga episode
765 dated here by applying simultaneously the Rb-Sr, Sm-Nd and Pb-Pb methods on various
766 leachates and residues of silicified carbonated rocks points to a wide regional extend. The
767 $^{40}Ar/^{39}Ar$ age at 2,673 ± 3 Ma of a barite from the same locality as the rocks studied here was
768 reported by De Ronde et al. (1991) with a release temperature of Ar at ca. 200°C. It
769 consolidates the thermal impact suggested by the positive Eu anomaly of the REE patterns.
770 However, the importance of this event does not exclude the potentiality of an even earlier
771 tectonic-thermal episode predicted by Hofmann (2005). It is significant in this respect, that

772 clay minerals separated from the same samples as those studied here provided a Sm-Nd
773 isochron age of 3,102 ± 64 Ma, while their Rb-Sr and K-Ar systems were affected later at
774 about 2.05 Ga (Toulkeridis et al., 1998). This younger 2.05 Ga age was obtained here by the
775 three methods, in fact between 2.07 and 2.45 Ga and mostly by data of leachates.
776 Interestingly, the older limit at 2.45 Ma obtained by a Rb-Sr isochron of sample FTG3
777 corresponds somewhat to $^{40}Ar/^{39}Ar$ ages of altered barite (De Ronde et al., 1991). The next
778 younger age at ~1.6 Ga was confirmed here by a Rb-Sr isochron of FTG1 aliquots, and as for
779 the event at 2.4 Ga, this age was set by $^{40}Ar/^{39}Ar$ ages of altered basalt pillows. (Layer et al.,
780 1992) that looks more as a local volcanic episode out of the regional context.
781
782 ## Conclusions
783
784 Based on a sequential leaching of silicified Archaean carbonates from Kaapvaal
785 Craton, the chemical data and Rb-Sr, Sm-Nd and Pb-Pb isotopic ages show that the
786 successive dilute HAc, HCl and $HNO_3$ acids interacted with soluble minerals of variable
787 chemical compositions. Application of the isotopic dating methods on the untreated, leached
788 and residual whole rocks also contributed to the reconstruction of the complex post-
789 depositional evolution of these Archaean rock-forming minerals. Already published isotopic
790 ages of 2.7 $\pm$ 0.1 and 2.3 $\pm$ 0.2 Ga were obtained again by combining the various leachates
791 and/or residues resulting from different reagents. These leachates also yielded a systematic
792 positive Eu anomaly and, therefore, resulted from large-scale fluid movements generated by
793 wide regional tectonic-thermal activities during the two dated events. Multiple analyses of
794 solid and soluble aliquots generate sometimes multiple sub-parallel isotopic trends tentatively
795 identified as isotrends with constitutive data points that are slightly more scattered than those
796 of the associated isochrons, confirming in turn age values within the analytical uncertainties
797 of the associated isochrons.
798 The younger event set here at about 1.6 $\pm$ 0.1 Ga could relate to the emplacement of
799 the Bushveld complex and/or other intrusive complexes of the Kaapvaal Craton. Similar ages
800 that probably represent closure temperatures of the Fig Tree sediments at about 200°C and
801 less, correspond to identical REE distribution patterns that were already reported elsewhere in
802 and around the craton.
803
804 ## Acknowledgments

Sadly, our co-author and friend Alfred passed away on May the 22nd, 2019. He contributed to this study long ago and we wanted to thank him, memorize his help and somehow honor his continuous sharing and ever-lasting interest for our work in isotope geochemistry. We would also like to take this opportunity to express thanks to many individuals who contributed to this long-term episode. Among those are P. Karcher, J. Samuel, B. Kiefel and D. Tisserand (CGS-CNRS/ULP, Strasbourg), E. Mackiolzyk (Max-Planck-Institut at Mainz) and N. Groshopf (University of Mainz) for technical assistance. The senior author would also like to thank Donald R. Lowe and Christoph E. Heubeck for introduction into the Barberton geology, Daniel M. Sigman and Gary Byerly for field assistance, and Gerhard van der Westhuizen for his generous hospitality in Barberton. Thanks are also dedicated for the logistic support provided by the Anglo–Vaal Corporation at Barberton, especially to Hilton G. Philpot, Stephanie McAulay and Marcus Tomkinson, as well as to the Anglo–American, Nelspruit for support especially by Marc Pryor. Financial support by the Deutsche Forschungsgemeinschaft (DFG) to T.T. and A.K. (Grant Kr-590/34) and by the German-French exchange program "Programme de Coopération Scientifique" to T.T, A.K. and N.C. is also gratefully acknowledged. At last and certainly not at least, sincere thanks are also dedicated to one of the anonymous reviewers who did a though reviewing work that deserves to be highlighted.

## References

Allsopp, H.L., Viljoen, M.J. and Viljoen, R.P. (1973) Strontium isotopic studies of the mafic and felsic rocks of the Onverwacht Group of the Swaziland Sequence. *Geologische Rundschau*, 62, 902-917.

Anhaeusser, C.R. (1973) The evolution of the early Precambrian crust of southern Africa. *Philosophical Transactions of the Royal Society of London*, A, 273, 359-388.

Anhaeusser, C.R. (2006) A reevaluation of Archean intracratonic terrane boundaries on the Kaapvaal Craton, South Africa: Collisional suture zones? *Geological Society of America Special Papers*, 405, 193-210.

Anhaeusser, C.R. (2014) Archaean greenstone belts and associated granitic rocks – A review. *Journal of African Earth Sciences*, 100, 684-732.

837 Anhaeusser, C.R. and Robb, L.J. (1981) Magmatic cycles and the evolution of the Archean
838 granitic crust in the eastern Transvaal and Swaziland. *Special Publication of the*
839 *Geological Society of Australia*, 7, 457-467.
840 Armstrong, R.A., Compston, W., De Wit, M.J. and Williams, I.S. (1990) The stratigraphy of
841 the 3.5-3.2 Ga Barberton Greenstone Belt revisited: a single zircon ion microprobe study.
842 *Earth and Planetary Science Letters*, 101, 90-106.
843 Babinski, M., Van Schmus, W.R. and Chemale, Jr., F. (1999) Pb–Pb dating and Pb isotope
844 geochemistry of Neoproterozoic carbonate rocks from the São Francisco basin, Brazil:
845 implications for the mobility of Pb. *Chemical Geology,* 160, 175-199.
846 Barton, J.M. Jr., Robb, I.J., Anhaeusser, C.R. and Van Nierop, D.A. (1983) Geochronologic
847 and Sr-isotopic studies of certain units in the Barberton granit-greenstone terrane, South
848 Africa. *Special Publication of the Geological Society of South Africa*, 9, 63-72.
849 Bau, M. (1991) Rare-earth element mobility during hydrothermal and metamorphic fluid-rock
850 interaction and the significance of the oxidation state of europium. *Chemical Geology*, 93,
851 219-230.
852 Bellefroid, E. J., Planavsky, N. J., Miller, N. R., Brand, U. and Wang, C. (2018) Case studies
853 on the utility of sequential carbonate leaching for radiogenic strontium isotope
854 analysis. *Chemical Geology*, 497, 88-99.
855 Bischoff, J.L. and Fitzpatrick, J.A. (1991) U-series dating of impure carbonates: an isochron
856 technique using total-sample dissolution. *Geochimica et Cosmochimica Acta*, 55, 543-554.
857 Bofinger, V.M., Compston, W. and Vernon, M.J. (1968) The application of acid leaching to
858 the Rb-Sr dating of a middle Ordovician shale. *Geochimica et Cosmochimica Acta*, 32,
859 823-833.
860 Bolhar, R., Hofmann, A., Woodhead, J., Hergt, J. and Dirks, P.H.G.M. (2002) Pb-and Nd-
861 isotope systematics of stromatolitic limestones from the 2.7 Ga Ngezi Group of the
862 Belingwe Greenstone Belt: constraints on timing of deposition and
863 provenance. *Precambrian Research*, 114, 277-294.
864 Bolhar, R., Kamber, B.S., Moorbath, S., Fedo, C.M. and Whitehouse, M.J. (2004)
865 Characterisation of early Archaean chemical sediments by trace element signatures. *Earth*
866 *and Planetary Science Letters* 222, 43-60.
867 Brooks, C., Hart, S.R., and Wendt, I. (1972) Realistic use of two-error regression treatments
868 as applied to Rubidium-Strontium data. *Reviews of Geophysics and Space Physics*, 10,
869 551-577.

870 Bros, R., Stille, P., Gauthier-Lafaye, F., Weber, F. and Clauer, N. (1992) Sm-Nd isotopic
871 dating of Proterozoic clay material: an example from the Francevillian sedimentary series,
872 Gabon. *Earth and Planetary Science Letters*, 113, 207-218.
873 Cameron, A.E., Smith, D.H. and Walker, R.L. (1969) Mass spectrometry of nanogram-size
874 samples of lead. *Analytical Chemistry,* 41, 525-526.
875 Chaudhuri, S. and Brookins, D.G. (1979) The Rb-Sr systematics in acid-leached clay
876 minerals. *Chemical Geology*, 24, 231-242.
877 Clauer, N. (1981) Rb-Sr and K-Ar dating of Precambrian clays and glauconies. *Precambrian*
878 *Research*, 15, 331-352.
879 Clauer, N., Chaudhuri, S., Kralik, M. and Bonnot-Courtois, C. (1993) Effects of experimental
880 leaching on Rb-Sr and K-Ar isotopic systems and REE contents of diagenetic illite.
881 *Chemical Geology*, 103, 1-16.
882 Clauer, N. and Chaudhuri, S. (2012) *Clays in crustal environments: Isotope dating and*
883 *tracing*. Springer Science & Business Media.
884 Cutts, K.A., Stevens, G., Hoffmann, J.E., Buick, I.S., Frei, D. and Münker, C. (2014) Paleo-to
885 Mesoarchean polymetamorphism in the Barberton Granite-Greenstone Belt, South Africa:
886 Constraints from U-Pb monazite and Lu-Hf garnet geochronology on the tectonic
887 processes that shaped the belt. *Geological Society of America Bulletin*, 126*,* 251-270.
888 Danielson, A., Möller, P. and Dulski, P. (1992) The europium anomalies in banded iron
889 formations and the thermal history of the oceanic crust. *Chemical Geology*, 97, 89-100.
890 Davidson, J., Charlier, B., Hora, J.M. and Perlroth R. (2005) Mineral isochrones and isotopic
891 fingerprints: Pitfalls and promises. *Geology*, 33, 29-32.
892 Decker, N.B., Byerly, G.R., Stiegler, M.T., Lowe, D.R. and Stefurak, E. (2015) High
893 resolution tephra and U/Pb chronology of the 3.33–3.26 Ga Mendon Formation, Barberton
894 Greenstone Belt, South Africa. *Precambrian Research*, 261, 54-74.
895 De Ronde, C.E.J., Hall, C.M., York, D. and Spooner, E.T.C. (1991) Laser step-heating
896 $^{40}Ar/^{39}Ar$ age spectra from early Archean (~3.5 Ga) Barberton greenstone belt sediments:
897 A technique for detecting cryptic tectono-thermal events. *Geochimica et Cosmochimica*
898 *Acta, 55*, 1933-1951.
899 De Ronde, C.E.J. and de Wit, M.J. (1994) Tectonic history of the Barberton greenstone belt,
900 South Africa: 490 million years of Archean crustal evolution. *Tectonics*, 13, 983-1005.
901 de Vries, S.T., Nijman, W. and Armstrong, R.A. (2006) Growth-fault structure and
902 stratigraphic architecture of the Buck Ridge volcano-sedimentary complex, upper

903 Hooggenoeg Formation, Barberton Greenstone Belt, South Africa. *Precambrian Research*,
904 149, 77-98.
905 de Wit, M.J., Furnes, H. and Robins, B. (2011) Geology and tectonostratigraphy of the
906 Onverwacht Suite, Barberton greenstone belt, South Africa. *Precambrian Research*, 186,
907 1-27.
908 Doe, R.B. (1970) Lead isotopes. Springer Verlag, Berlin, Heidelberg, and New York, 137pp.
909 Drabon, N., Galić, A., Mason, P.R. and Lowe, D.R. (2019) Provenance and tectonic
910 implications of the 3.28–3.23 Ga Fig Tree Group, central Barberton greenstone belt, South
911 Africa. *Precambrian Research*, 325, 1-19.
912 Erel, Y., Harlavan, Y., Stein, M. and Blum, J.D. (1997) U-Pb dating of Fe-rich phases using a
913 sequential leaching method. *Geochimica et Cosmochimica Acta*, 61, 1697-1703.
914 Eriksson, K.A., Krapez, B. and Fralick, P.W. (1994) Sedimentology of Archean greenstone
915 belts: signatures of tectonic evolution. *Earth Science Reviews,* 37, 1-88.
916 Eriksson, K.A. and Simpson, E. (2000) Quantifying the oldest tidal record: The 3.2 Ga
917 Moodies Group, Barberton Greenstone Belt, South Africa. *Geology*, 28, 831-834.
918 Evensen N.M., Hamilton P.J., and O'Nions, R.K. (1978) Rare-earth abundances in chondritic
919 meteorites. *Geochimica et Cosmochimica Acta,* 42, 1199-1212.
920 Fölling, P.G., Zartman, R.E. and Frimmel, H.E. (2000) A novel approach to double-spike Pb–
921 Pb dating of carbonate rocks: examples from Neoproterozoic sequences in southern Africa.
922 *Chemical Geology*, 171, 97-122.
923 Furnes, H., de Wit, M. and Robins, B. (2013) A review of new interpretations of the
924 tectonostratigraphy, geochemistry and evolution of the Onverwacht Suite, Barberton
925 Greenstone Belt, South Africa. *Gondwana Research*, 23, 403-428.
926 Gromet, L.P., Dymek, R.F., Haskin, L.A. and Korotev, R.L. (1984) The North American
927 Shale Composite – Its compilation, major and trace element characteristics. *Geochimica*
928 *et Cosmochimica Acta*, 48, 2469-2482.
929 Grosch, E.G., Kosler, J., McLoughlin, N., Drost, K., Slama, J. and Pedersen, R.B. (2011)
930 Paleoarchean detrital zircon ages from the earliest tectonic basin in the Barberton
931 Greenstone Belt, Kaapvaal craton, South Africa. *Precambrian Research*, 191, 85-99.
932 Grosch, E.G., Vidal, O., Abu-Alam, T. and McLoughlin, N. (2012) P–T Constraints on the
933 metamorphic evolution of the paleoarchean Kromberg type-section, Barberton greenstone
934 belt, South Africa. *Journal of Petrology*, 53, 513-545.

935 Heinrichs, T.K. and Reimer, T. (1977) A sedimentary barite deposit from the Archean Fig
936 Tree Group of the Barberton Mountain Land (South Africa). *Economic Geology*, 72,
937 1426–1441.
938 Hessler, A.M. and Lowe, D.R. (2006) Weathering and sediment generation in the Archean: an
939 integrated study of the evolution of siliciclastic sedimentary rocks of the 3.2 Ga Moodies
940 Group, Barberton Greenstone Belt, South Africa. *Precambrian Research*, 151, 185-210.
941 Heubeck, C. (2009) An early ecosystem of Archean tidal microbial mats (Moodies Group,
942 South Africa, ca. 3.2 Ga). *Geology*, 37, 931-934.
943 Heubeck, C. and Lowe, D.R. (1994) Late syndepositional deformation and detachment
944 tectonics in the Barberton Greenstone Belt, South Africa. *Tectonics*, 13, 1514-1536.
945 Heubeck, C., Engelhardt, J., Byerly, G. R., Zeh, A., Sell, B., Luber, T. and Lowe, D.R. (2013)
946 Timing of deposition and deformation of the Moodies Group (Barberton Greenstone Belt,
947 South Africa): Very-high-resolution of Archaean surface processes. *Precambrian*
948 *Research*, 231, 236-262.
949 Hofmann, A. (2005) The geochemistry of sedimentary rocks from the Fig Tree Group,
950 Barberton greenstone belt: implications for tectonic, hydrothermal and surface processes
951 during mid-Archaean times. *Precambrian Research*, 143, 23-49.
952 Hofmann, A. and Bolhar, R. (2007) Carbonaceous cherts in the Barberton greenstone belt and
953 their significance for the study of early life in the Archean record. *Astrobiology*, 7, 355-
954 388.
955 Hofmann, A., Bolhar, R., Orberger, B. and Foucher, F. (2013) Cherts of the Barberton
956 Greenstone Belt, South Africa: Petrology and trace element geochemistry of 3.5 to 3.3 Ga
957 old silicified volcaniclastic sediments. *South African Journal of Geology*, 116, 297-322.
958 Jahn, B.M., Bertrand-Sarfati, J., Morin, N. and Mace, J. (1990) Direct dating of stromatolitic
959 carbonates from the Schmidtsdrif Formation (Transvaal Dolomite), South Africa, with
960 implications on the age of the Ventersdorp Supergroup. *Geology*, 18, 1211-1214.
961 Jahn, B.M. and Cuvellier, H. (1994) Pb-Pb and U-Pb geochronology of carbonate rocks: an
962 assessment. *Chemical Geology*, 115, 125-151.
963 Kamo, S.L. and Davis, D.W. (1993) Reassessment of Archean crustal development in the
964 Barberton Mountain Land, South Africa, based on U-Pb dating. *Tectonics*, 13, 167-192.
965 Kato, Y., Kawakami, T., Kano, T., Kunugiza K. and Swamy, N.S. (1996) Rare-earth element
966 geochemistry of banded iron formations and associated amphibolite from the Sargur belts,
967 south India. *Journal of Southeast Asian Earth Sciences*, 14, 161-164.

968 Kaurova, O.K., Ovchinnikova, G.V. and Gorokhov, I.M. (2010) U-Th-Pb systematics of
969 Precambrian carbonate rocks: dating of the formation and transformation of carbonate
970 sediments. *Stratigraphy and Geological Correlation*, 18, 252-268.
971 Krogh, T.E. (1973) A low-contamination method for hydrothermal decomposition of zircon
972 and extraction of U and Pb for isotopic age determinations. *Geochimica et Cosmochimica*
973 *Acta*, 9, 1-32.
974 Kröner, A., Byerly, G.R. and Lowe, D.R. (1991) Chronology of early Archean granite-
975 greenstone evolution in the Barberton Mountain Land, South Africa, based on precise
976 dating by single zircon evaporation. *Earth and Planetary Science Letters*, 103, 41-54.
977 Kröner, A. and Todt, W. (1988) Single zircon dating constraining the maximum age of the
978 Barberton greenstone belt, southern Africa. *Journal of Geophysical Research*, 93, 15329-
979 15337.
980 Lana, C., Buick, I., Stevens, G., Rossouw, R. and De Wet, W. (2011) 3230–3200 Ma post-
981 orogenic extension and mid-crustal magmatism along the southeastern margin of the
982 Barberton Greenstone Belt, South Africa. *Journal of Structural Geology*, 33, 844-858.
983 Layer, P.W., Kröner, A. and York, D. (1992) Pre-3000 Ma thermal history of the Archean
984 Kaap Valley pluton, South Africa. *Geology*, 20, 717-720.
985 Lécuyer, C., Gruau, G., Anhaeusser, C.R. and Fourcade, S. (1994) The origin of fluids and the
986 effects of metamorphism on the primary chemical compositions of Barberton komatiites:
987 New evidence from geochemical (REE) and isotopic (Nd, O, H, $^{39}Ar/^{40}Ar$) data.
988 *Geochimica et Cosmochimica Acta*, 58, 969-984
989 Lopez-Martinez, M.D., York, D. and Hanes, J.A. (1992) A $^{40}Ar/^{39}Ar$ geochronological study
990 of komatiites and komatiitic basalts from the lower Onverwacht volcanics: Barberton
991 Mountain Land, South Africa. *Precambrian Research*, 57, 91-119.
992 Lowe, D.R. (1991) Geology of the Barberton Greenstone Belt: an overview. In: L.D. Ashwal
993 (Ed.), Two Cratons and an Orogen – Excursion guidebook and review articles for a field
994 workshop through selected Archean terranes of Swaziland, South Africa and Zimbabwe.
995 *IGCP Project 280*, Department of Geology, University of the Witwatersrand, South
996 Africa, 47-58.
997 Lowe, D.R. and Byerly, G.R. (2007) An overview of the geology of the Barberton Greenstone
998 Belt and vicinity: implications for early crustal development. In: M.J. van Kranendonk,
999 R.H. Smithies and V.H. Bennett (Editors), Earth's Oldest Rocks, 15, *Developments in*
1000 *Precambrian Geology*, 15, 481–526.

1001 Lowe, D.R. and Nocita, B.W. (1999) Foreland basin sedimentation in the Mapepe Formation,
1002 southern-facies Fig Tree Group: In: Eds. D.R. Lowe and G.R. Byerly, Geologic Evolution
1003 of the Barberton Greenstone Belt, South Africa. *Geological Society of America Special*
1004 *Paper*, 329, 233-258.
1005 Ludwig, K.R. (2003) User's Manual for Isoplot/Ex Version 2.02. A geochronological Toolkit
1006 for Microsoft Excel, Berkeley Geochronology Center, Special Publication 1a, Berkeley,
1007 CA, USA.
1008 Luo, S. and Ku, T.L. (1991) U-series isochron dating: A generalized method employing total-
1009 sample dissolution. *Geochimica et Cosmochimica Acta*, 55, 555-564.
1010 McIntyre, G.A., Brooks, C., Compston, C. and Turek, A.,1(966) The statistical assessment of
1011 Rb-Sr isochrons. *Journal of Geophysical Research*, 71, 5459-5468.
1012 McLennan, S.M., Taylor, S.R. and Kröner, A. (1983) Geochemical evolution of Archean
1013 shales from South Africa. I. The Swaziland and Pongola Supergroups. *Precambrian*
1014 *Research*, 22, 93-124.
1015 MacRae, N.D., Nesbitt, H.W. and Kronberg, B.I. (1992) Development of a positive Eu
1016 anomaly during diagenesis. *Earth Planetary Science Letters,* 109, 3-4.
1017 Melezhik, V.A., Gorokhov, I.M., Kuznetsov, A.B. and Fallick, A.E. (2001)
1018 Chemostratigraphy of Neoproterozoic carbonates: implications for 'blind dating'. *Terra*
1019 *Nova*, 13, 1-11.
1020 Moorbath, S., Taylor, P.N., Orpen, J.L., Treloar, P. and Wilson, J.F. (1987) First direct
1021 radiometric dating of Archaean stromatolitic limestone. *Nature*, 326, 865-867.
1022 Morton, J.P. and Long, L.E. (1980) Rb-Sr dating of Paleozoic glauconite from the Llano
1023 region, central Texas. *Geochimica et Cosmochimica Acta*, 44, 663-671.
1024 Nakada, R., Shibuya, T., Suzuki, K. and Takahashi, Y.( 2017) Europium anomaly variation
1025 under low-temperature water-rock interaction: A new thermometer. *Geochemistry*
1026 *International*, 55, 822–832.
1027 Poujol, M., Robb, L.J., Anhaeusser, C.R. and Gericke, B. (2003) A review of the
1028 geochronological constraints on the evolution of the Kaapvaal Craton, South Africa.
1029 *Precambrian Research*, 127, 181-213.
1030 South African Committee for Stratigraphy (SACS) (1980) Stratigraphy of South Africa: Part
1031 I: Lithostratigraphy of the Republic of South Africa, South West Africa/Namibia and the
1032 Republics of Bophuthatswana, Transkai, and Venda. *Geological Survey of South Africa*,
1033 Handbook, 8, 690p.

1034 Sahuquillo, A., Rigol, A. and Rauret, G. (2003) Overview of the use of leaching/extraction
1035 tests for risk assessment of trace metals in contaminated soils and sediments. *Trends in*
1036 *Analytical Chemistry*, 22, 152-159.
1037 Samuel, J., Rouault, R. and Besnus, Y. (1985) Analyse multi-élémentaire standardisée des
1038 matériaux géologiques en spectrométrie d'émission par plasma à couplage inductif.
1039 *Analusis,* 13, 312-317.
1040 Schaltegger, U., Stille, P., Rais, N., Piqué, A. and Clauer, N. (1994) Nd and Sr isotopic dating
1041 of diagenesis and low-grade metamorphism of argillaceous sediments: *Geochimica et*
1042 *Cosmochimica Acta*, 58, 1471-1481.
1043 Schidlowski, M., Eichmann, R. and Junge, C.E. (1975) Precambrian sedimentary carbonates:
1044 carbon and oxygen isotope geochemistry and implications for the terrestrial oxygen
1045 budget. *Precambrian Research*, 22 1-69.
1046 Schwarcz, H.P. and Latham, A.G. (1989) Dirty calcites 1. Uranium-series dating of
1047 contaminated calcite using leachates alone. *Chemical Geology, Isotope Geoscience*
1048 *Section*, 80, 35-43.
1049 Shields, G. and Veizer, J. (2002) Precambrian marine carbonate isotope database: Version
1050 1.1. *Geochemistry, Geophysics, Geosystems*, 3, 1031. doi: 10.1029/2001GC000266.
1051 Stevens, G. and Moyen, J.F. (2007) Metamorphism in the Barberton Granite Greenstone
1052 Terrain: a record of Paleoarchean accretion. Earth's Oldest Rocks. *Developments in*
1053 *Precambrian Geology*, 15, 669-698.
1054 Taylor, S.R. and McLennan, S.M. (1985) The continental crust: Its Composition and
1055 Evolution. *Blackwell, Malden*, Mass., 312 p.
1056 Tice, M.M., Bostick, B.C. and Lowe, D.R. (2004) Thermal history of the 3.5–3.2 Ga
1057 Onverwacht and Fig Tree Groups, Barberton greenstone belt, South Africa, inferred by
1058 Raman microspectroscopy of carbonaceous material. *Geology*, 32, 37-40.
1059 Todt, W., Cliff, R.A., Hanser, A. and Hofmann, A.W. (1996) Evaluation of a $^{202}Pb/^{205}Pb$
1060 double spike for high-precision lead isotope analysis. Earth Processes: Reading the
1061 isotopic code. Eds. Basu, A. and Hart, S., *Geophysical Monograph Series*, 95, 429-437.
1062 Toulkeridis, T., Goldstein, S.L., Kröner, A., Clauer, N., Lowe, D.R., Todt, W. and
1063 Schidlowski, M.( 1998) Sm-Nd, Rb-Sr, Pb-Pb dating of carbonates from the early
1064 Archaean Barberton Greenstone Belt, South Africa: evidence for post-depositional isotopic
1065 resetting at low temperature. *Precambrian Research,* 92, 129-144.

1066 Toulkeridis, T., Clauer, N., Kröner, A., Reimer, T. and Todt, W. (1999) Characterization,
1067 provenance, and tectonic setting of Fig Tree greywackes from the Archaean Barberton
1068 greenstone belt, South Africa. *Sedimentary Geology*, 124 113-129.
1069 Toulkeridis, T., Peucker-Ehrenbrink, B., Schidlowski, M., Kröner, A., Todt, W. and Clauer,
1070 N. (2010) A chemical and isotopic study of Archaean magnesite, Barberton Greenstone
1071 Belt, South Africa. *Journal of the Geological Society of London*, 167, 943-952.
1072 Toulkeridis, T., Clauer, N., Kröner, A. and Todt, W. (2015) Mineralogy, geochemistry and
1073 isotopic dating of shales from the Barberton Greenstone Belt, South Africa: Provenance
1074 and tectonic implications. *South African Journal of Geology*, 118, 389-410.
1075 Van Kranendonk, M. J., Kröner, A., Hegner, E., and Connelly, J. (2009) Age, lithology and
1076 structural evolution of the c. 3.53 Ga Theespruit Formation in the Tjakastad area,
1077 southwestern Barberton Greenstone Belt, South Africa, with implications for Archaean
1078 tectonics. *Chemical Geology*, 261, 115-139.
1079 Veizer, J., Hoefs, J., Lowe, D.R. and Thurston, P.C. (1989) Geochemistry of Precambrian
1080 carbonates: II. Archean greenstone belts and Archean seawater. *Geochimica et*
1081 *Cosmochimica Acta*, 53, 859-871.
1082 Viljoen, M.J. and Viljoen, R.P. (1969) An introduction to the geology of the Barberton
1083 granite-greenstone terrain. *Geological Society of South Africa Special Publication*, 2, 9-28.
1084 Wabo, H., Maré, L.P., Beukes, N.J., Kruger, S.J., Humbert, F. and de Kock, M.O. (2018)
1085 Mineral transformations during thermal demagnetization of sideritic jasper mesobands in
1086 jaspilites of the ~3.25 Ga Fig Tree Group in the Barberton Greenstone Belt, Kaapvaal
1087 craton (South Africa). *South African Journal of Geology*, 121, 131-140.
1088 Wang, W., Bolhar, R., Zhou, M.F. and Zhao, X.F. (2018) Enhanced terrestrial input into
1089 Paleoproterozoic to Mesoproterozoic carbonates in the southwestern South China Block
1090 during the fragmentation of the Columbia supercontinent. *Precambrian Research*, 313, 1-
1091 17.
1092 Weill, D.F. and Drake M.J. (1973) Europium Anomaly in Plagioclase Feldspar: Experimental
1093 Results and Semiquantitative Model. *Science*, 180, 1059-1069.
1094 Weis, D. and Wasserburg, G.J. (1987) Rb-Sr and Sm-Nd isotope geochmistry of cherts from
1095 the Onverwacht Group (3.5 AE), South Africa. *Geochimica et Cosmochimica Acta*, 51,
1096 973-984.
1097 Westall, F., De Ronde, C.E., Southam, G., Grassineau, N., Colas, M., Cockell, C. and
1098 Lammer, H. (2006) Implications of a 3.472–3.333 Gyr-old subaerial microbial mat from
1099 the Barberton greenstone belt, South Africa for the UV environmental conditions on the

early Earth. *Philosophical Transactions of the Royal Society of London* B: Biological Sciences, 361: 1857-1876.

White, W.M. and Patchett, J. (1984) Hf-Nd-Sr isotopes and incompatible element abundances in island arcs: implications for magma origins and crust-mantle evolution. *Earth and Planetary Science Letters*, 67, 167-185.

Zeh, A., Gerdes, A. and Millonig, L. (2011) Hafnium isotope record of the Ancient Gneiss Complex, Swaziland, southern Africa: evidence for Archaean crust–mantle formation and crust reworking between 3.66 and 2.73 Ga. *Journal of the Geological Society*, 168, 953-964.

Zeh, A., Gerdes, A. and Heubeck, C. (2013) U–Pb and Hf isotope data of detrital zircons from the Barberton Greenstone Belt: constraints on provenance and Archaean crustal evolution. *Journal of the Geological Society*, 170, 215-223.

Zhao, B., Clauer, N., Robb, L. J., Zwingmann, H., Toulkeridis, T. and Meyer, F.M. (1999) K-Ar dating of white micas from the Ventersdorp Contact Reef of the Witwatersrand Basin, South Africa: timing of post-depositional alteration. *Mineralogy and Petrology*, 66, 149-170.

## Figure and Table captions

**Figure 1:** Sample location near the city of Barberton within the Barberton Greenstone Belt (after Toulkeridis et al., 1998). The central map is located as a rectangle on the sketch of South Africa in the upper left corner with the states of Swaziland and Lesotho. The red star locates the sampling places. The dashed line to the right is the boundary between the South African Transvaal and the Swaziland.

**Figure 2:** The Ca/Si, Mg/Si and Fe/Si ratios of the successive $H_2O$, HAc, HCl and $HNO_3$ leachates from studied samples. The different colors of the symbols represent the different types of leachates.

**Figure 3:** Scanning-electron microscopic pictures of the FTG samples; (A) idiomorphic dolomite crystals in the matrix of sample FTG1 surrounded by a fine-grained layer of illite-type crystals; (B) a barite-rich vein crosscutting sample FTG3; (C) a blow up of the FTG1 matrix with elongated illite and squared quartz crystals; (D) A blow-up of a dolomite crystal in the FTG1 matrix. The pictures A to C are from Toulkeridis et al. (1998).

**Figure 4:** Chondrite and PAAS normalized REE patterns of: (A) the untreated FTG whole rocks; (B) the FTG1 residues after each leaching step; (C) the FTG1 leachates after each

leaching step. Most duplicated residues and leachates being extremely similar, only one of each has been portrayed.

**Figure 5:** Rb-Sr patterns of the leachates and residues of the four FTG samples by the successive reagents. The four untreated whole-rock data are in red. The shapes and colors of the symbols stand for the four displays. The age values of the arrays are given along the respective alignments together with the initial ratios.

**Figure 6:** Sm-Nd patterns for the leachates and residues of the four FTG samples for the successive reagents. The shapes and colors of the symbols stand for the four displays. The age values of the arrays are given along the respective alignments.

**Figure 7:** Pb-Pb diagrams obtained by the interactions of the successive reagents identified by the same symbols in each display. The shape and color of the symbols stand for the four displays.

**Figure 8:** Two examples of Sm/Nd (in A) and Pb/Pb (in B) isotrends. The shape and color of the symbols stand for the two displays.

**Figure 9:** Rb-Sr diagrams of the leachates (in A and B) and of the untreated whole rocks (in C) of the four FTG samples. The diagram B is a blow up of display A. The colors of the symbol stand for the two A and B diagrams and the numbers in the three diagrams correspond to the samples.

**Figure 10:** Sm-Nd patterns of the leachates (A) and residues (B) of the four FTG samples identified by the colored symbols to the lower right side of the upper pattern. The symbol shapes and colors in the upper pattern correspond to the types of aliquots.

**Figure 11:** Rb-Sr displays of all residues in diagram (A) and those of the different residues (B1 to B4) of each FTG sample. The colored symbols and the numbers in the diagram (A) correspond to the four FTG samples. The symbols in the B diagrams correspond to the same aliquots.

**Table 1:** Calculated percentages of the leachates and the residues by the different reagents of the four Fig Tree samples. The indices a and b stand for the duplicate samples collected near the FGT1 sample.

**Table 2:** Ratios by weight of the major elements of the leachates obtained by the successively used $H_2O$, HAc, HCl and $HNO_3$ reagents on the four samples. The indices a and b stand for the duplicate samples collected near the FTG1 sample.

**Table 3:** Amounts of REEs leached off the four FTG samples by the successive reagents. The total contents are in μg/g.

**Table 4:** The rare-earth elemental contents of the leachates (labeled L) and residues (labeled R) after the successive HAc, HCl and $HNO_3$ leaching steps of the four samples. WR stands for whole rocks and the indices a and b of sample FTG1 stand for the duplicate samples collected nearby.

**Table 5:** The Rb-Sr and Sm-Nd isotopic data. WR corresponds to whole rocks, L to leachates and R to residues of each $H_2O$, HAc, HCl and $HNO_3$ reagent. The indices a and b stand for the duplicate samples collected near the sample FTG1.

**Table 6:** The Pb-Pb isotopic data with the $\pm 2\sigma$ uncertainties.

**Table 7:** A summary of the Rb-Sr, Sm-Nd and Pb-Pb age values obtained for the isochrons and isotrends of the four FTG samples. The numbers in brackets relate to independent age calculations for each method and sample, while leach stands for leachates. The numbers in bold stand for each major isochron result.

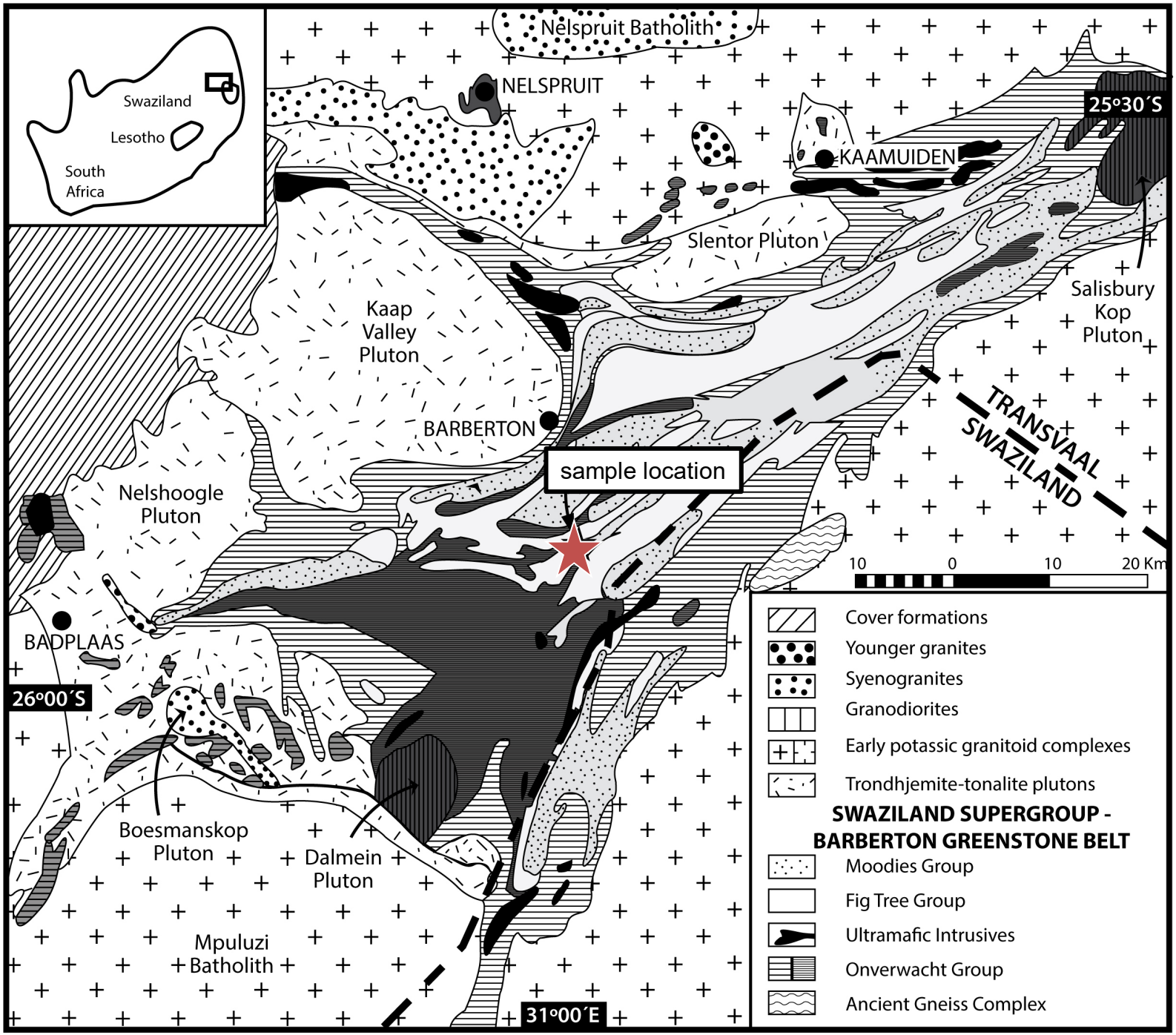
Swaziland
Lesotho
South Africa
Nelspruit Batholith
NELSPRUIT
25°30´S
KAAMUIDEN
Slentor Pluton
Salisbury Kop Pluton
Kaap Valley Pluton
BARBERTON
sample location
TRANSVAAL
SWAZILAND
Nelshoogle Pluton
10 0 10 20 Km
BADPLAAS
26°00´S
Boesmanskop Pluton
Dalmein Pluton
Mpuluzi Batholith
31°00´E
Cover formations
Younger granites
Syenogranites
Granodiorites
Early potassic granitoid complexes
Trondhjemite-tonalite plutons
SWAZILAND SUPERGROUP - BARBERTON GREENSTONE BELT
Moodies Group
Fig Tree Group
Ultramafic Intrusives
Onverwacht Group
Ancient Gneiss Complex

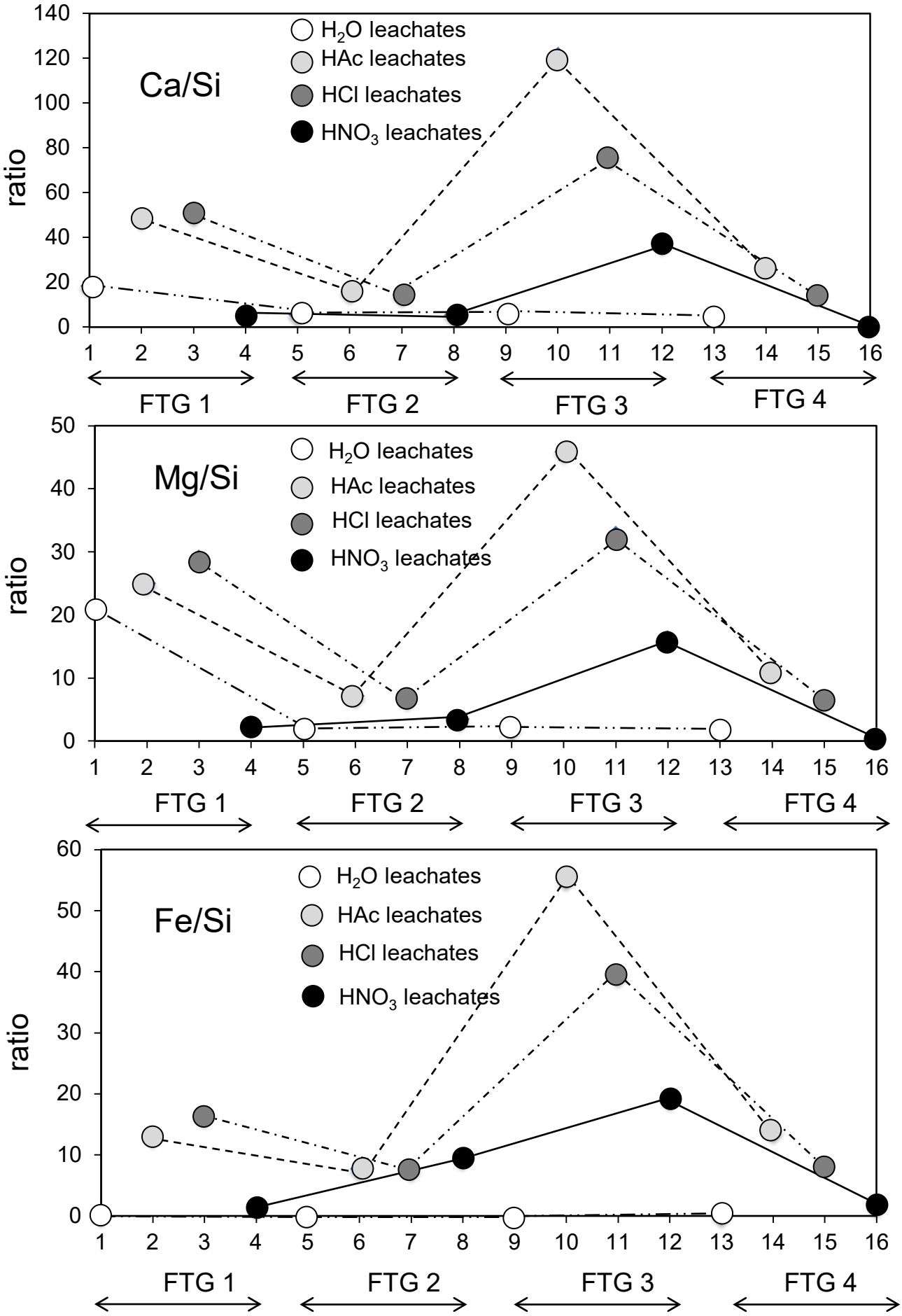
Ca/Si
ratio
$H_2O$ leachates
HAc leachates
HCl leachates
$HNO_3$ leachates
FTG 1
FTG 2
FTG 3
FTG 4
Mg/Si
ratio
$H_2O$ leachates
HAc leachates
HCl leachates
$HNO_3$ leachates
FTG 1
FTG 2
FTG 3
FTG 4
Fe/Si
ratio
$H_2O$ leachates
HAc leachates
HCl leachates
$HNO_3$ leachates
FTG 1
FTG 2
FTG 3
FTG 4

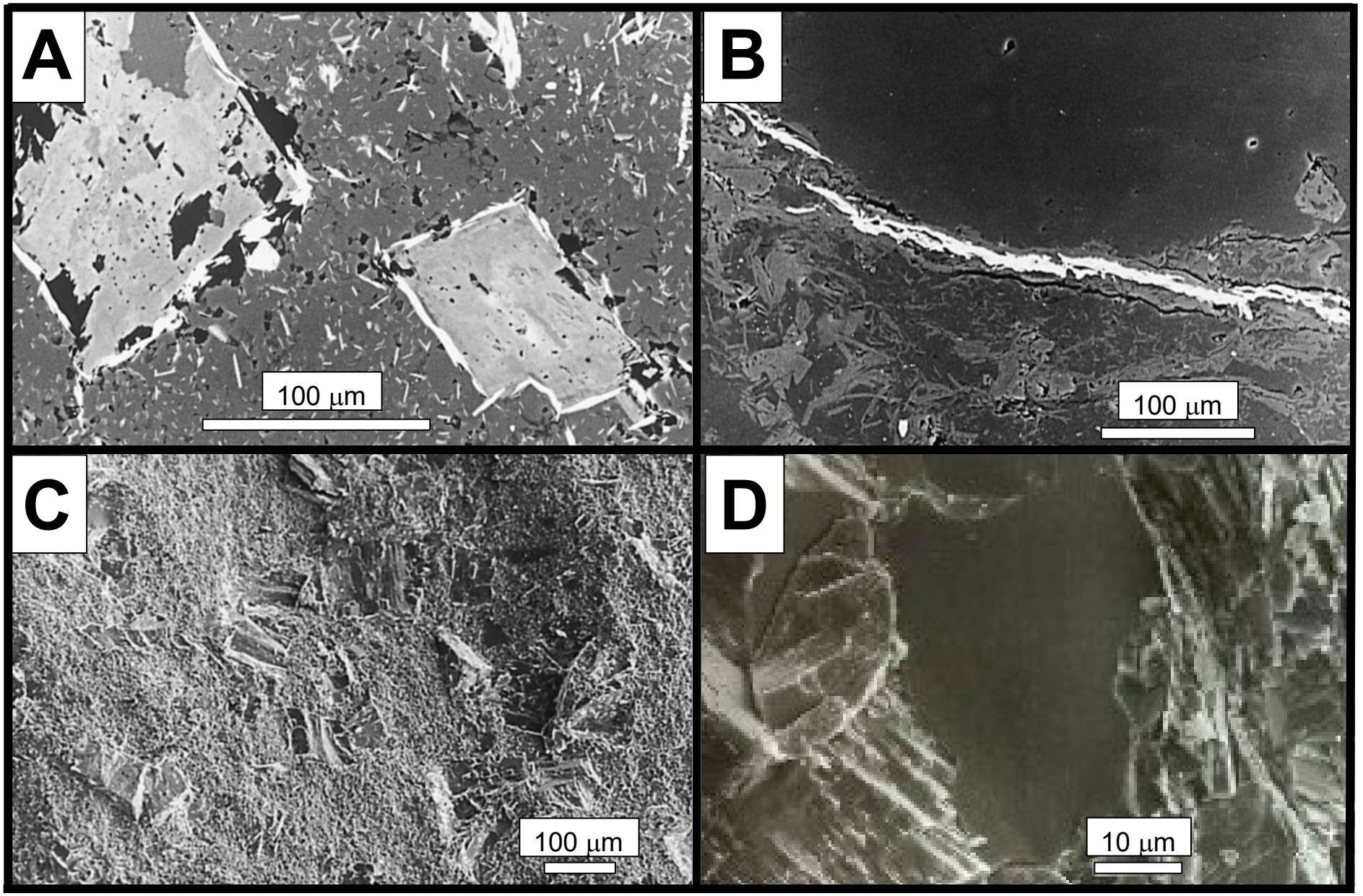
A
100 μm
B
100 μm
C
100 μm
D
10 μm

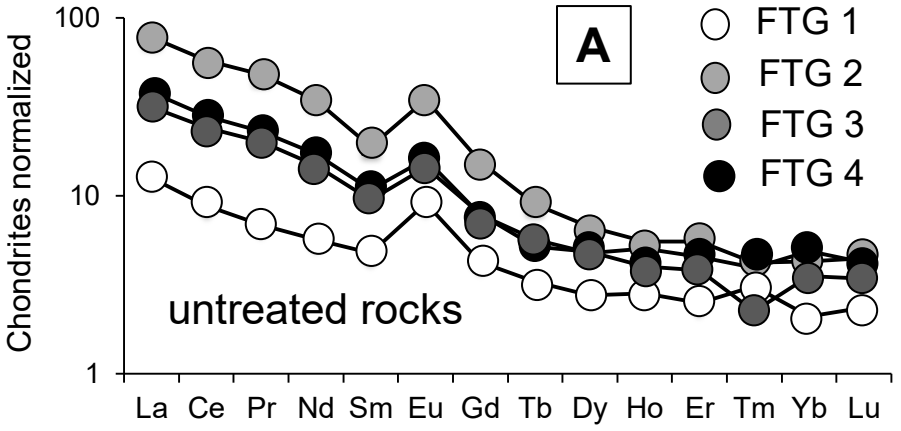
Chondrites normalized
100
10
1
A
FTG 1
FTG 2
FTG 3
FTG 4
untreated rocks
La Ce Pr Nd Sm Eu Gd Tb Dy Ho Er Tm Yb Lu

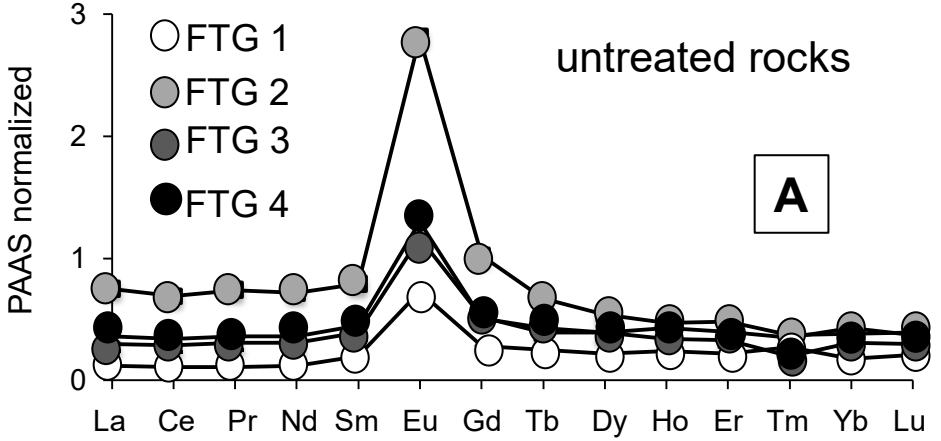
PAAS normalized
3
2
1
0
FTG 1
FTG 2
FTG 3
FTG 4
untreated rocks
A
La Ce Pr Nd Sm Eu Gd Tb Dy Ho Er Tm Yb Lu

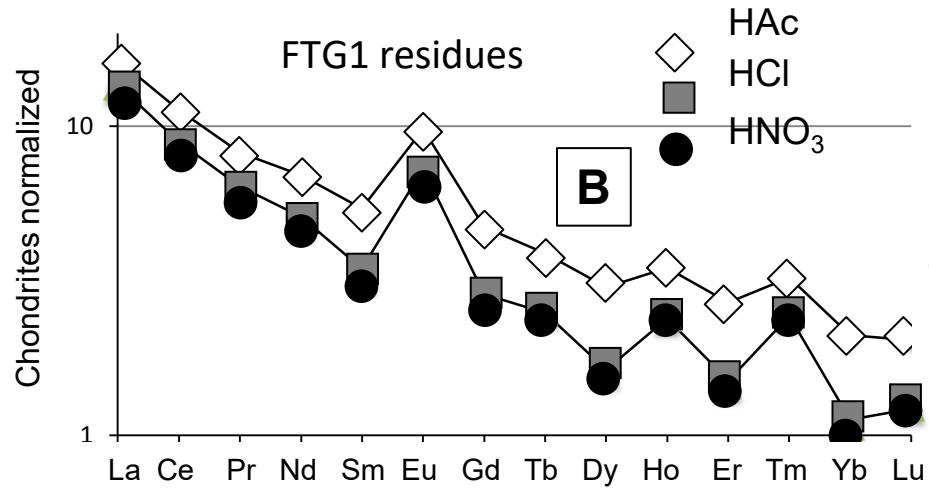
Chondrites normalized
10
1
FTG1 residues
HAc
HCl
HNO3
B
La Ce Pr Nd Sm Eu Gd Tb Dy Ho Er Tm Yb Lu

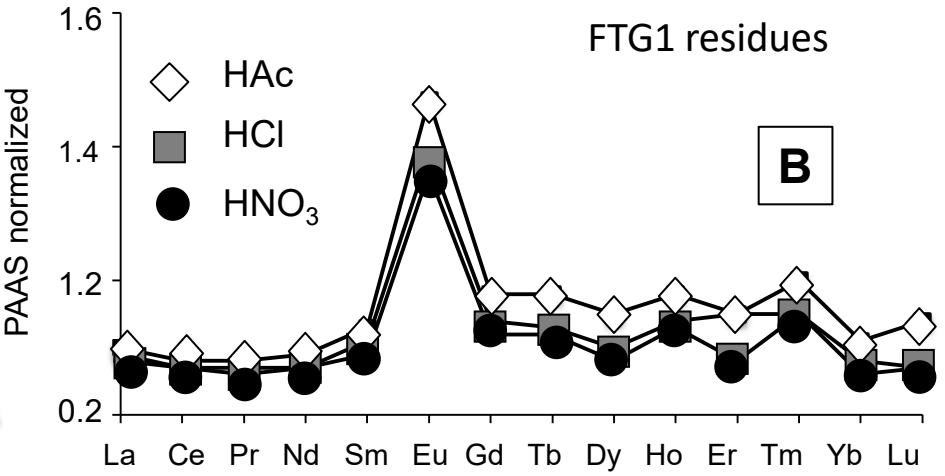
PAAS normalized
1.6
1.4
1.2
0.2
FTG1 residues
HAc
HCl
HNO3
B
La Ce Pr Nd Sm Eu Gd Tb Dy Ho Er Tm Yb Lu

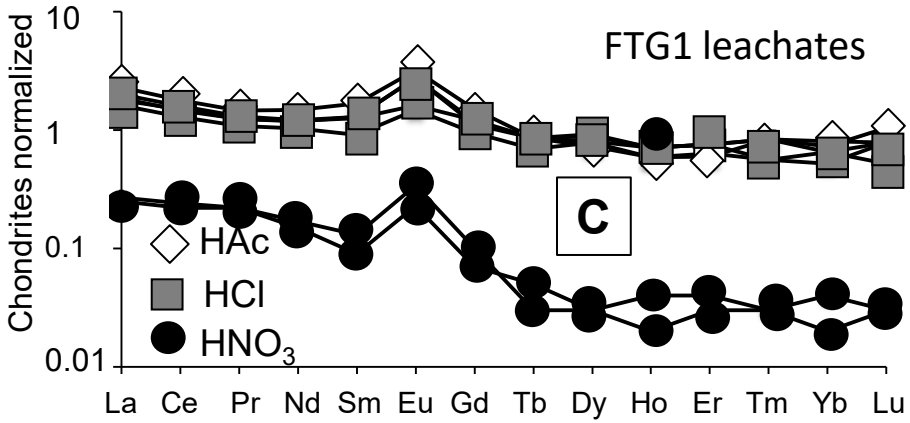
Chondrites normalized
10
1
0.1
0.01
FTG1 leachates
C
HAc
HCl
HNO3
La Ce Pr Nd Sm Eu Gd Tb Dy Ho Er Tm Yb Lu

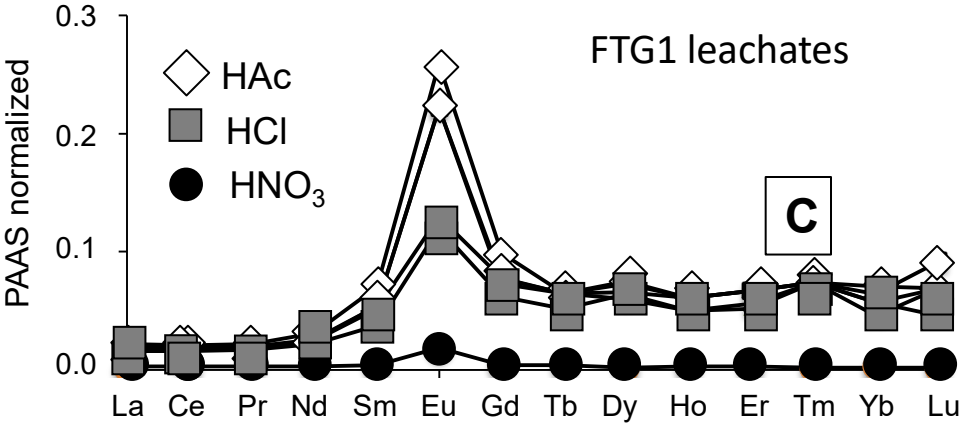
PAAS normalized
0.3
0.2
0.1
0.0
FTG1 leachates
HAc
HCl
HNO3
C
La Ce Pr Nd Sm Eu Gd Tb Dy Ho Er Tm Yb Lu

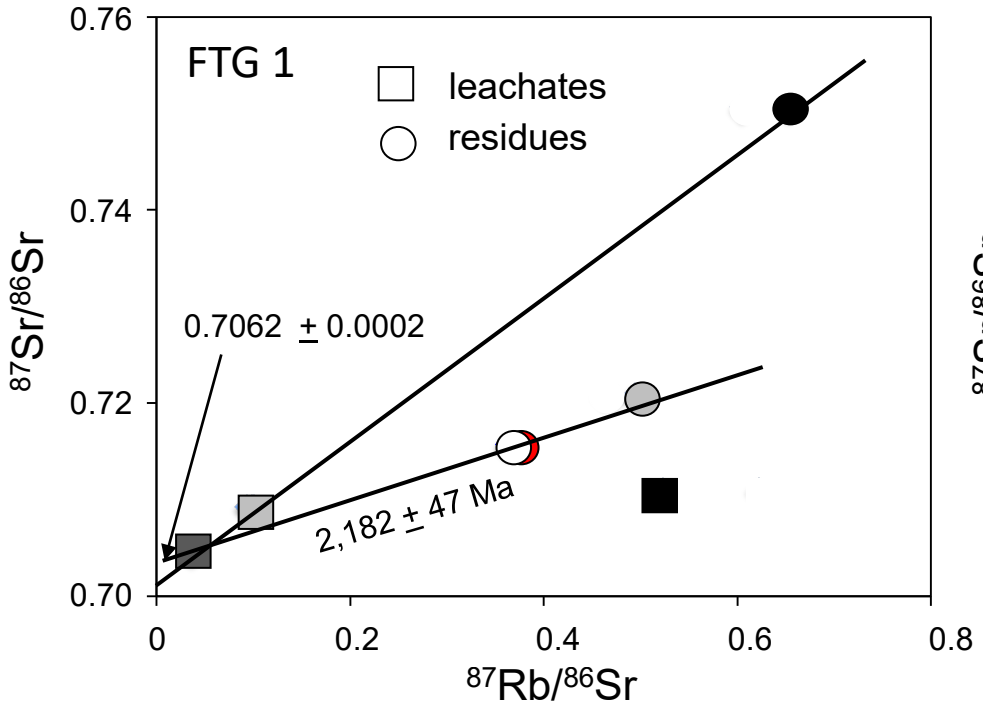
FTG 1
leachates
residues
0.7062 ± 0.0002
2,182 ± 47 Ma
0.76
0.74
0.72
0.70
0
0.2
0.4
0.6
0.8
87Sr/86Sr
87Rb/86Sr

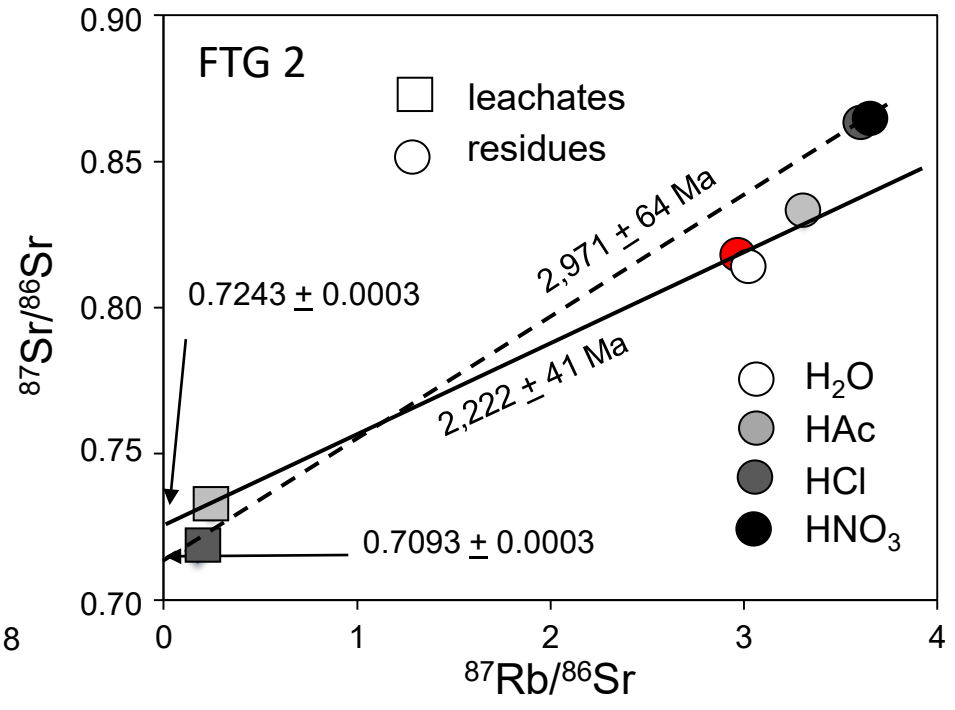
FTG 2
leachates
residues
0.7243 ± 0.0003
2,971 ± 64 Ma
2,222 ± 41 Ma
0.7093 ± 0.0003
H2O
HAc
HCl
HNO3
0.90
0.85
0.80
0.75
0.70
0
1
2
3
4
87Sr/86Sr
87Rb/86Sr

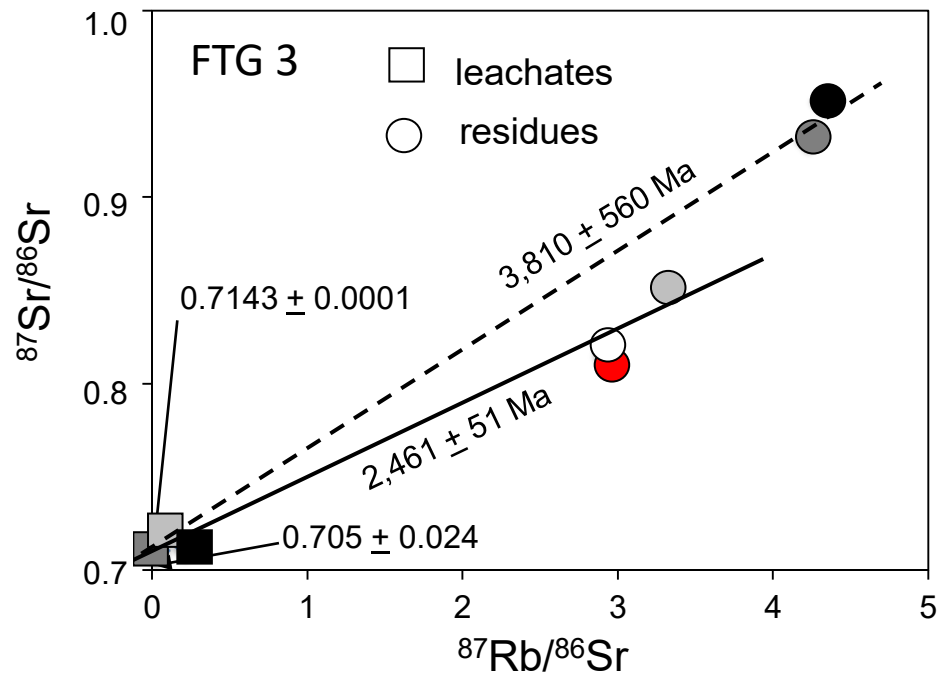
FTG 3
leachates
residues
0.7143 ± 0.0001
3,810 ± 560 Ma
2,461 ± 51 Ma
0.705 ± 0.024
1.0
0.9
0.8
0.7
0
1
2
3
4
5
87Sr/86Sr
87Rb/86Sr

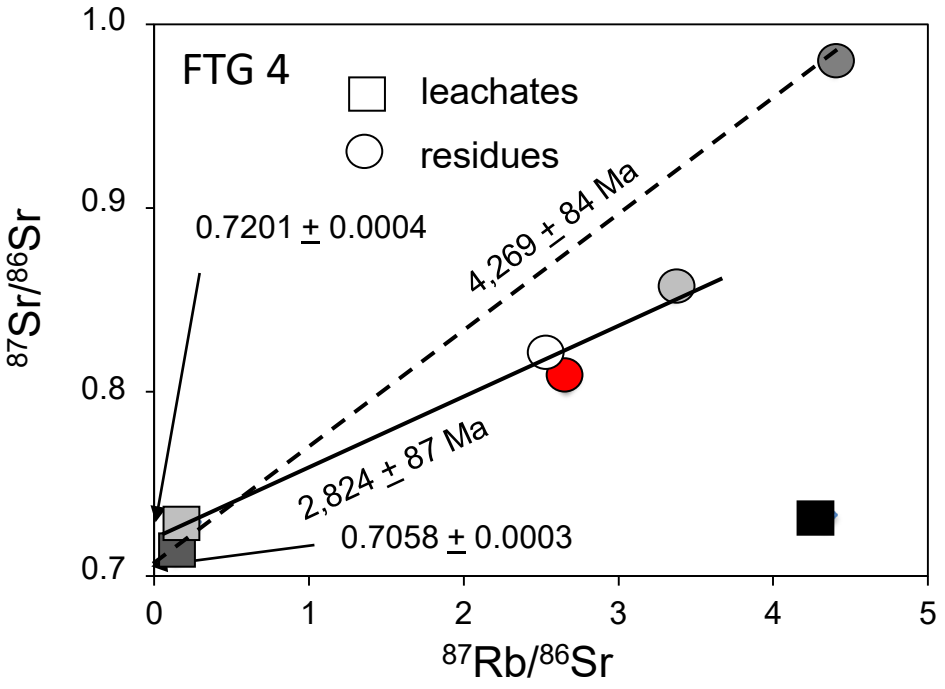
FTG 4
leachates
residues
0.7201 ± 0.0004
4,269 ± 84 Ma
2,824 ± 87 Ma
0.7058 ± 0.0003
1.0
0.9
0.8
0.7
0
1
2
3
4
5
87Sr/86Sr
87Rb/86Sr

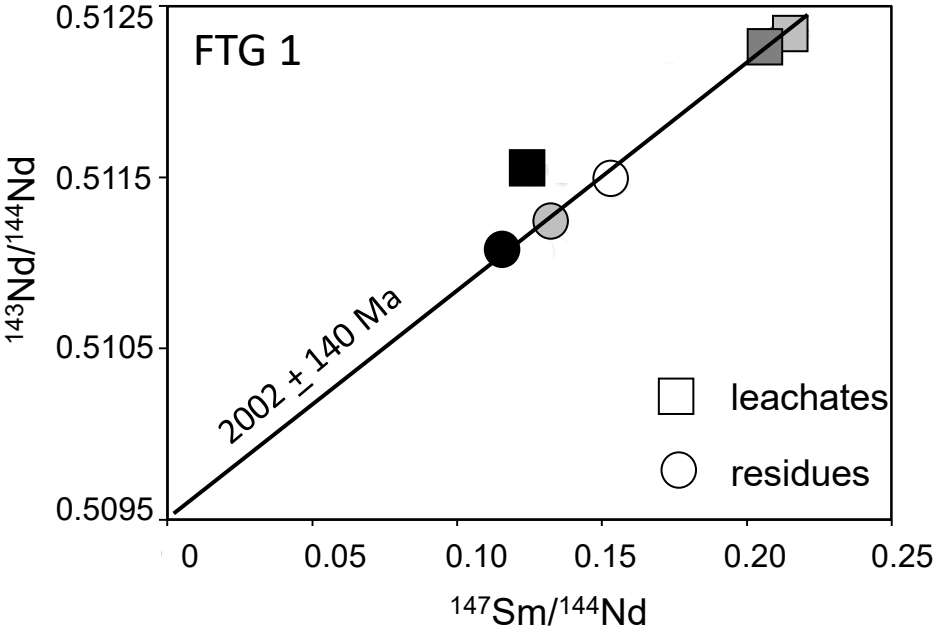
FTG 1
0.5125
0.5115
0.5105
0.5095
143Nd/144Nd
2002 ± 140 Ma
leachates
residues
0
0.05
0.10
0.15
0.20
0.25
147Sm/144Nd

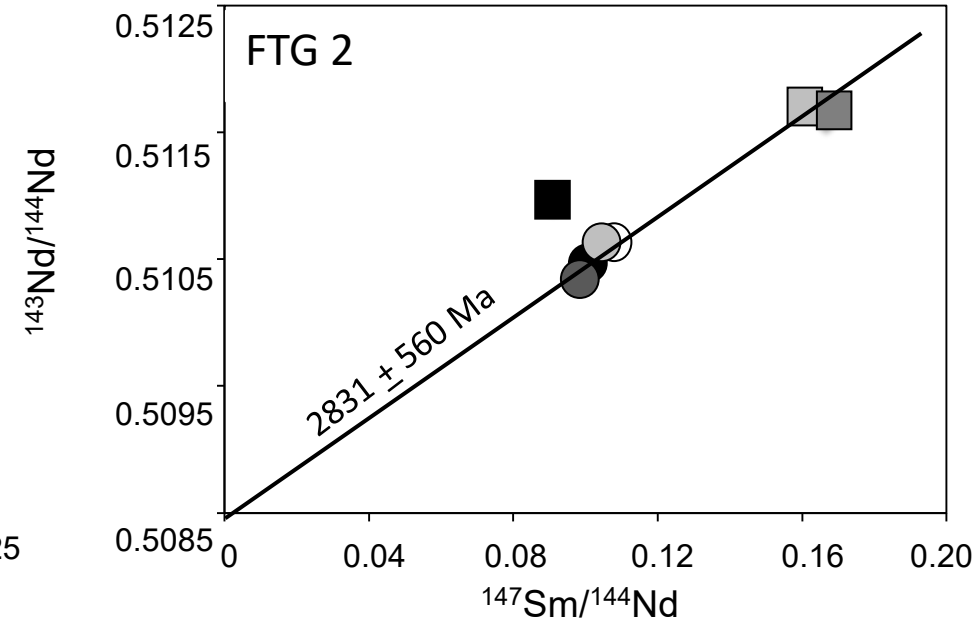
FTG 2
0.5125
0.5115
0.5105
0.5095
0.5085
143Nd/144Nd
2831 ± 560 Ma
0
0.04
0.08
0.12
0.16
0.20
147Sm/144Nd

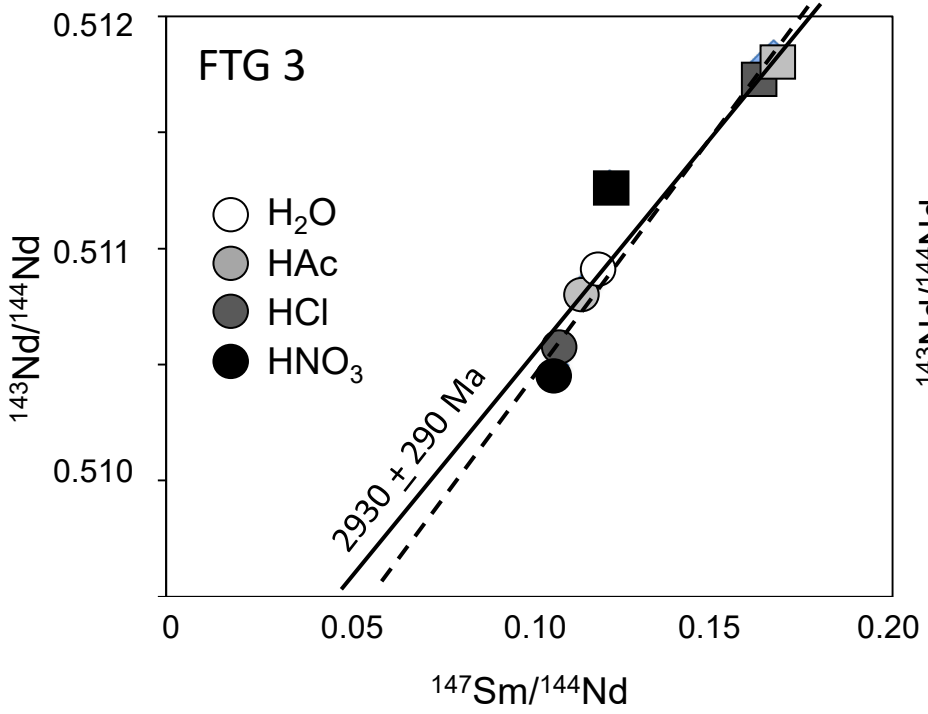
FTG 3
0.512
0.511
0.510
143Nd/144Nd
H2O
HAc
HCl
HNO3
2930 ± 290 Ma
0
0.05
0.10
0.15
0.20
147Sm/144Nd

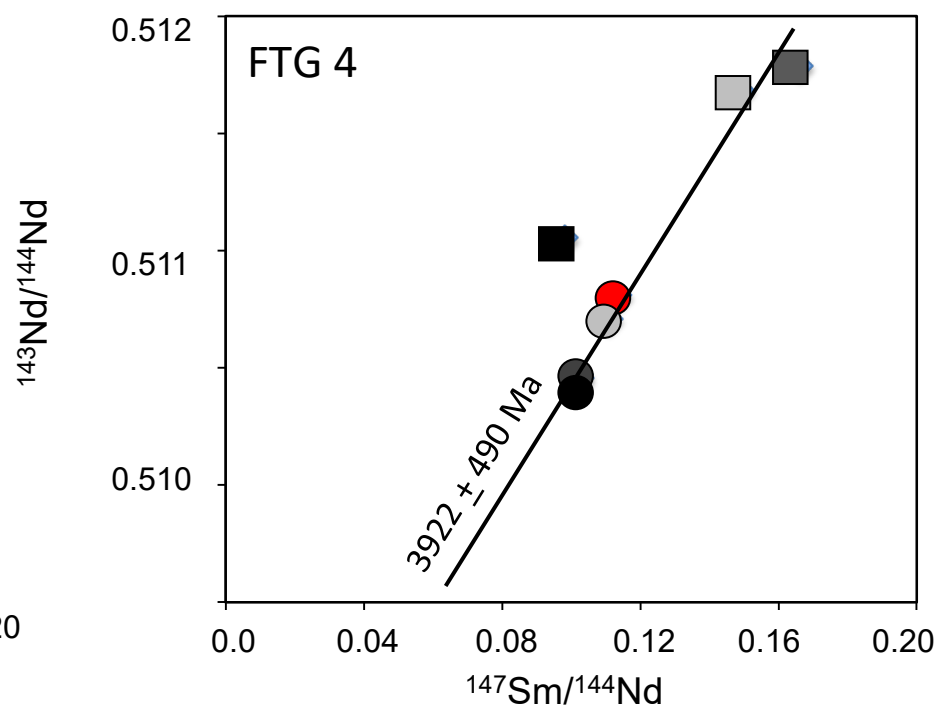
FTG 4
0.512
0.511
0.510
143Nd/144Nd
3922 ± 490 Ma
0.0
0.04
0.08
0.12
0.16
0.20
147Sm/144Nd

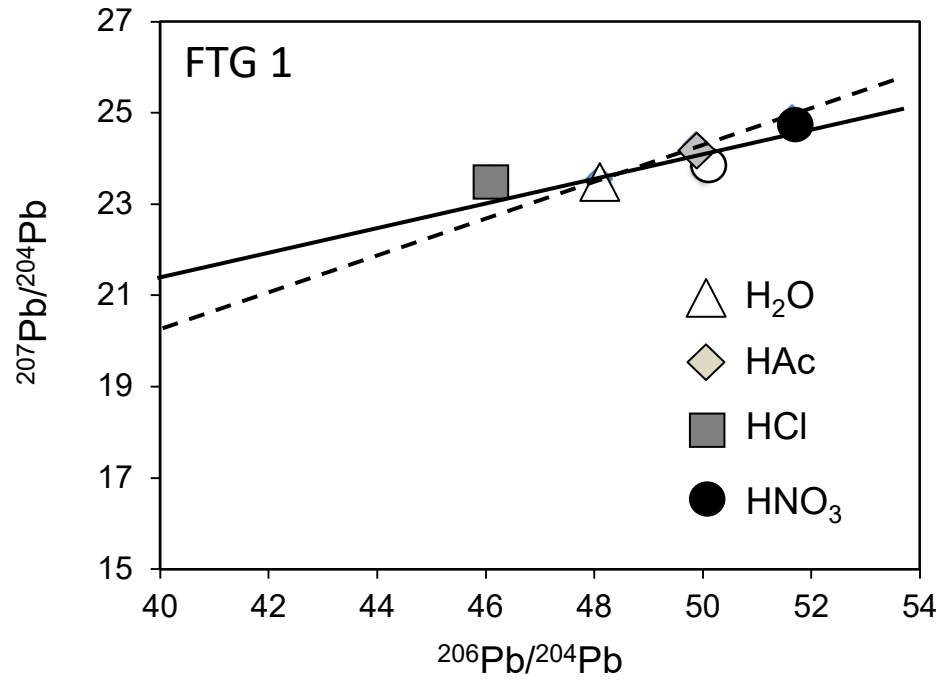
FTG 1
$^{207}Pb/^{204}Pb$
$^{206}Pb/^{204}Pb$
$H_2O$
HAc
HCl
$HNO_3$

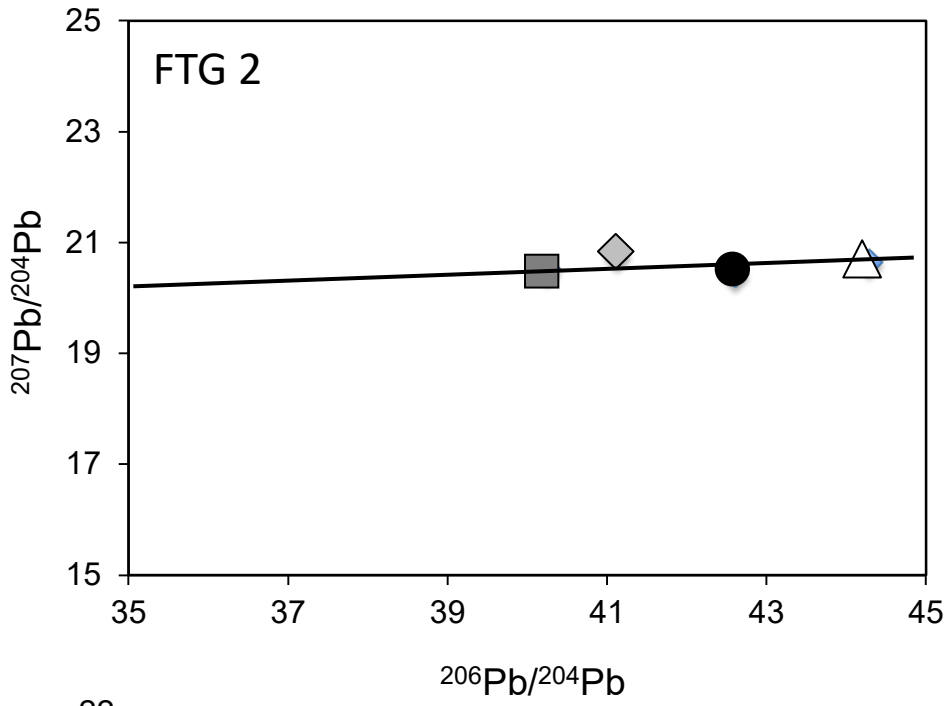
FTG 2
$^{207}Pb/^{204}Pb$
$^{206}Pb/^{204}Pb$

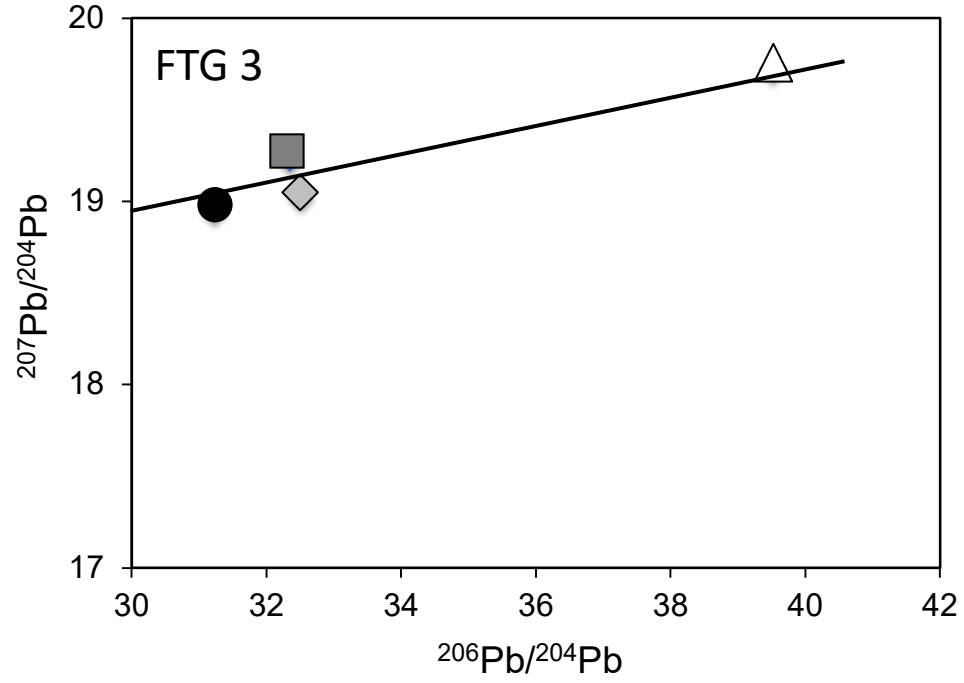
FTG 3
$^{207}Pb/^{204}Pb$
$^{206}Pb/^{204}Pb$

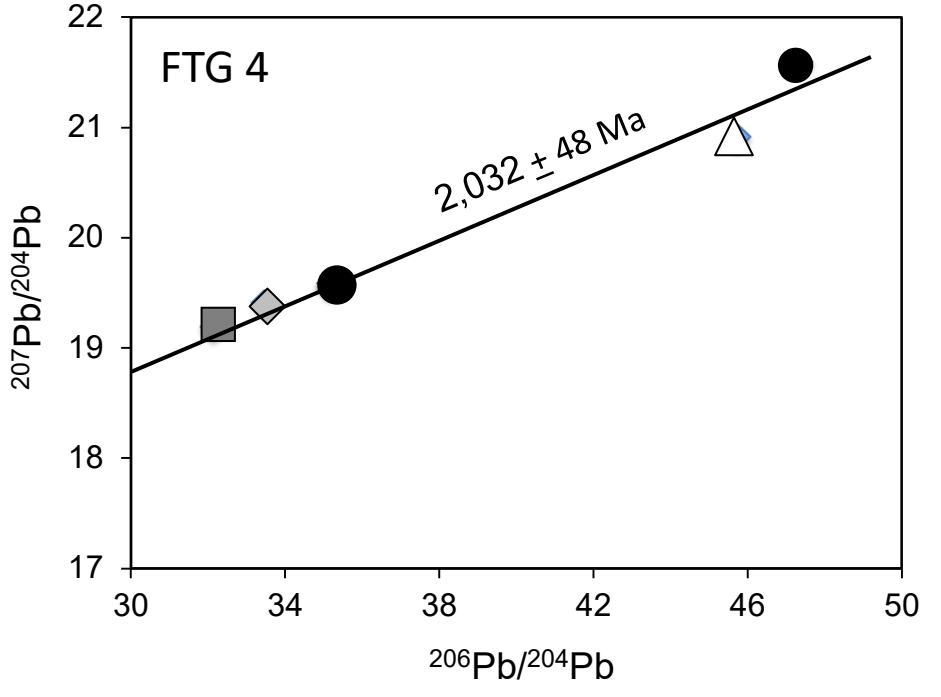
FTG 4
2,032 ± 48 Ma
$^{207}Pb/^{204}Pb$
$^{206}Pb/^{204}Pb$

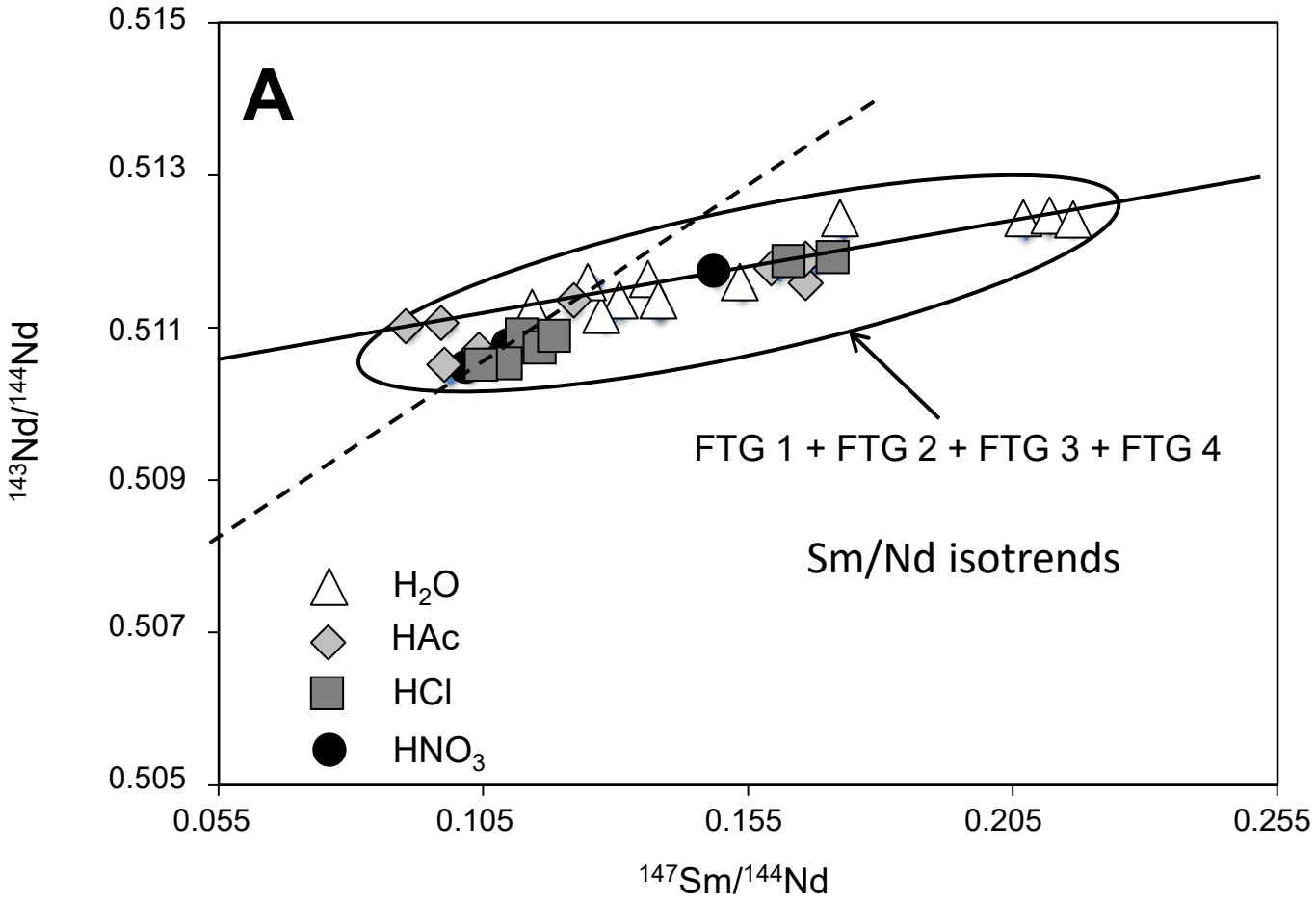
A
0.515
0.513
0.511
0.509
0.507
0.505
0.055
0.105
0.155
0.205
0.255
143Nd/144Nd
147Sm/144Nd
FTG 1 + FTG 2 + FTG 3 + FTG 4
Sm/Nd isotrends
H2O
HAc
HCl
HNO3

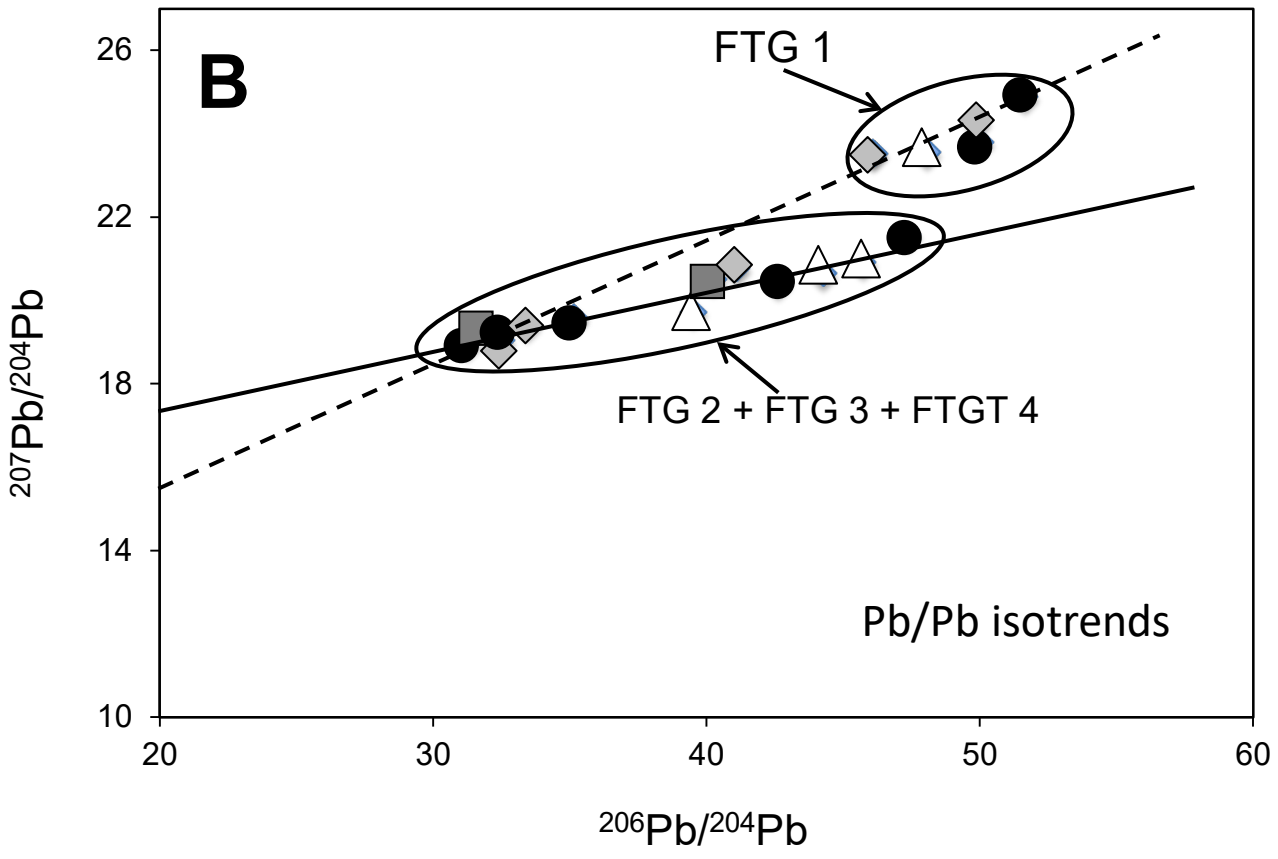
B
26
22
18
14
10
20
30
40
50
60
207Pb/204Pb
206Pb/204Pb
FTG 1
FTG 2 + FTG 3 + FTGT 4
Pb/Pb isotrends

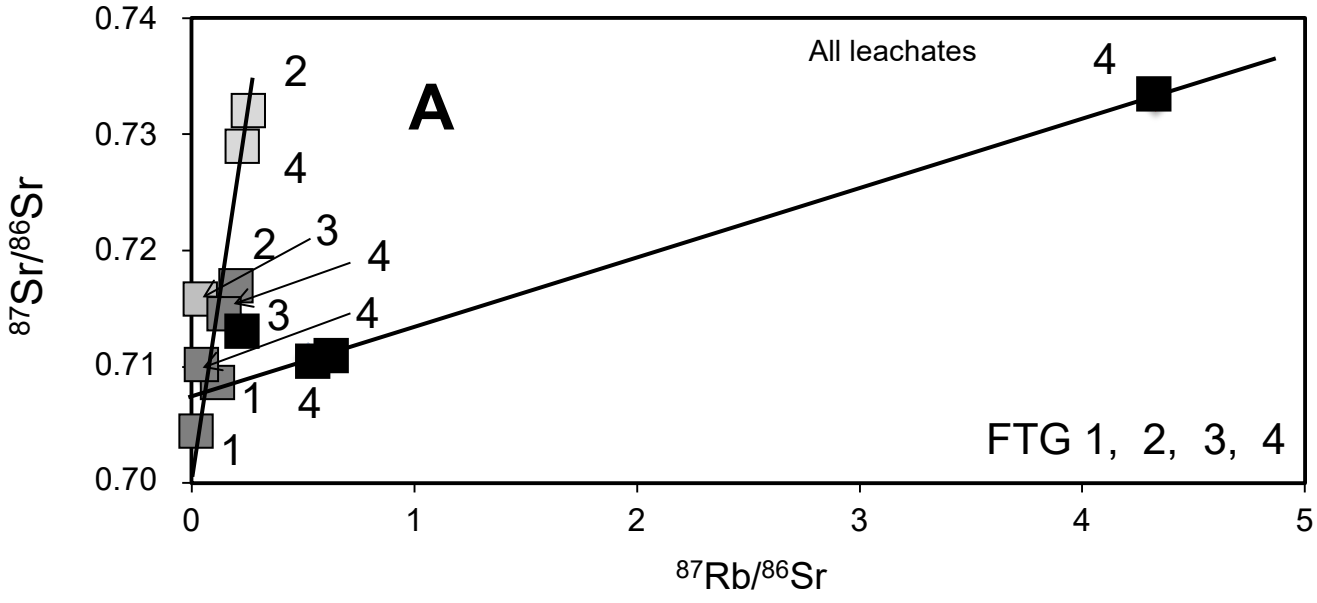
A
All leachates
FTG 1, 2, 3, 4
$^{87}Sr/^{86}Sr$
$^{87}Rb/^{86}Sr$
0.74
0.73
0.72
0.71
0.70
0
1
2
3
4
5

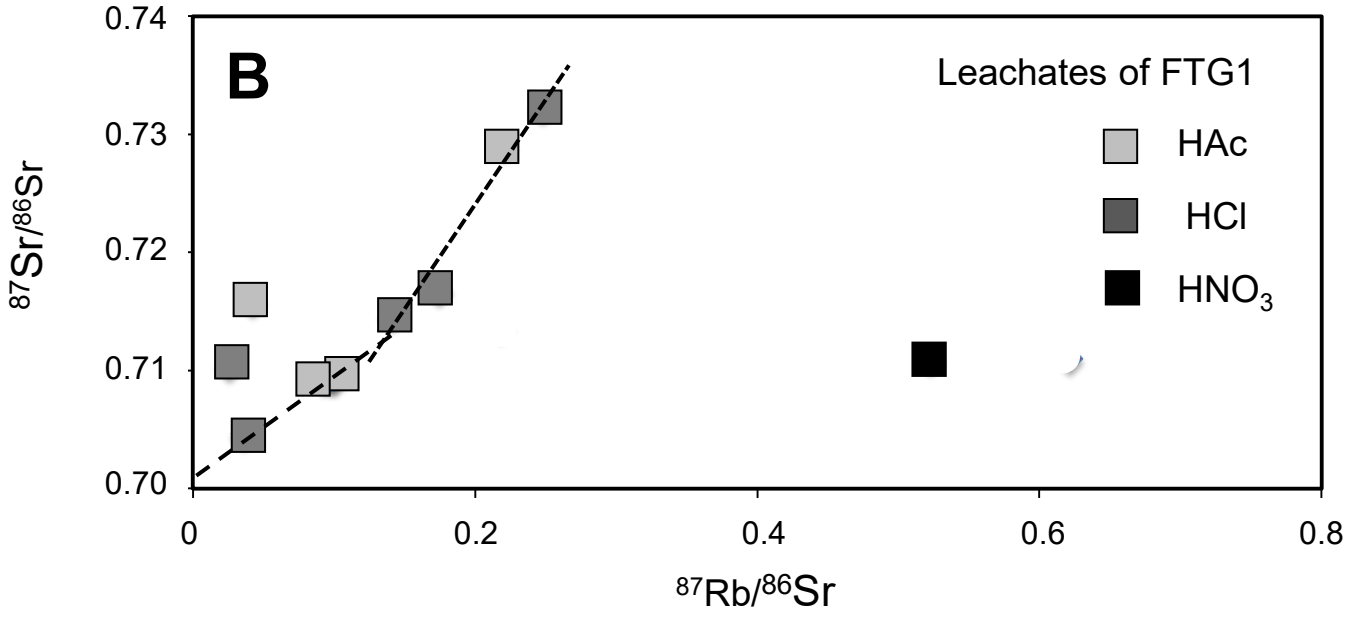
B
Leachates of FTG1
HAc
HCl
$HNO_3$
$^{87}Sr/^{86}Sr$
$^{87}Rb/^{86}Sr$
0.74
0.73
0.72
0.71
0.70
0
0.2
0.4
0.6
0.8

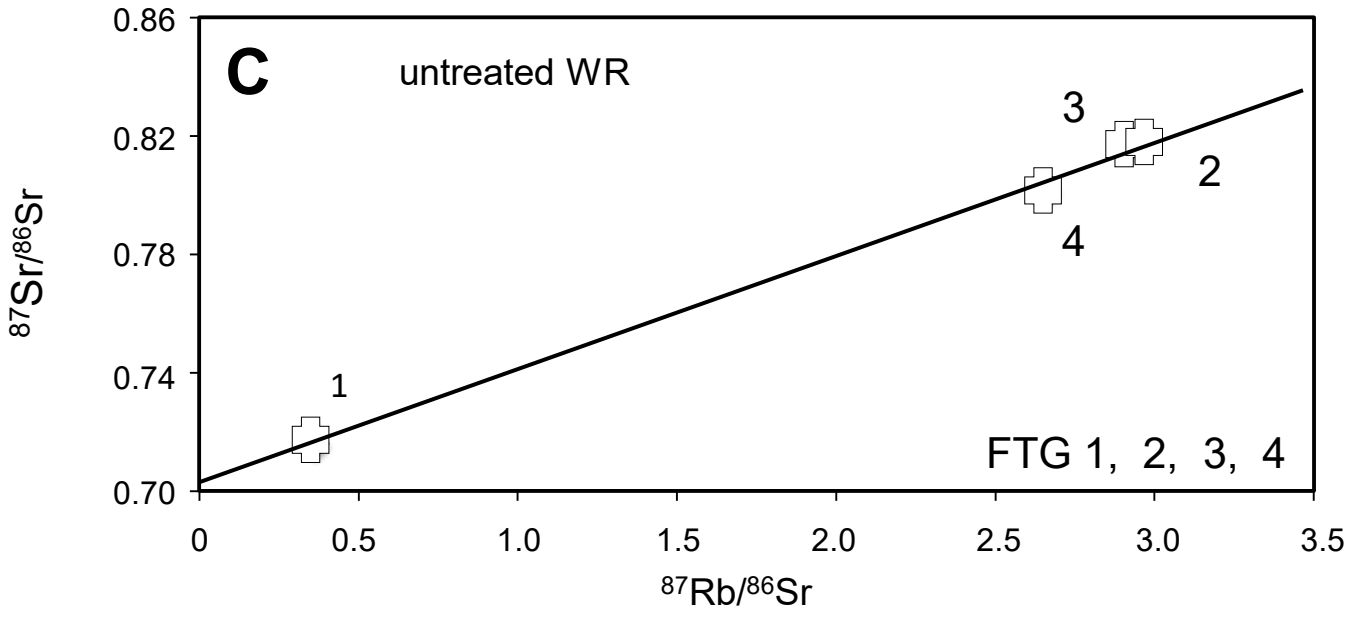
C
untreated WR
FTG 1, 2, 3, 4
$^{87}Sr/^{86}Sr$
$^{87}Rb/^{86}Sr$
0.86
0.82
0.78
0.74
0.70
0
0.5
1.0
1.5
2.0
2.5
3.0
3.5

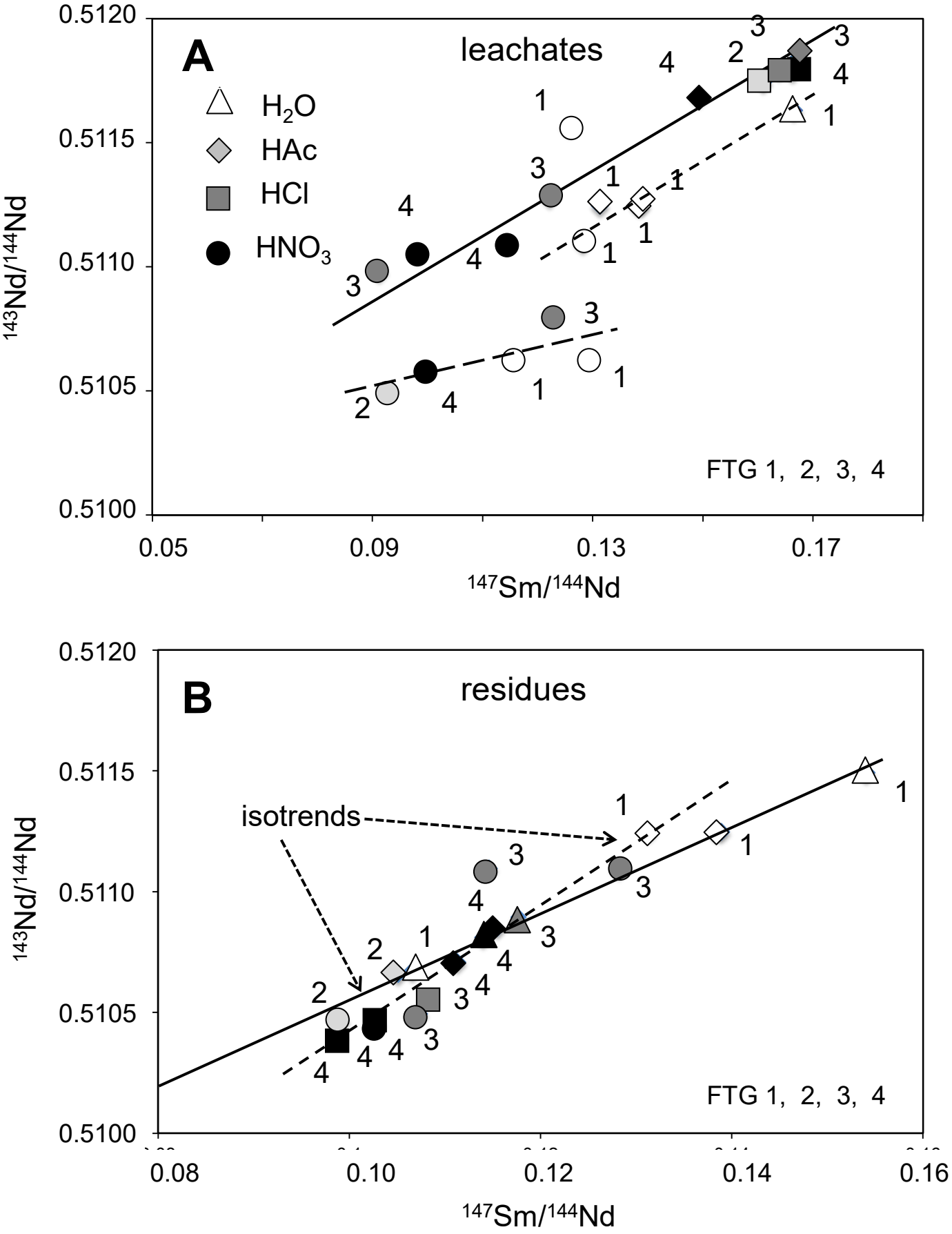
A
leachates
H2O
HAc
HCl
HNO3
FTG 1, 2, 3, 4
143Nd/144Nd
147Sm/144Nd
0.5120
0.5115
0.5110
0.5105
0.5100
0.05
0.09
0.13
0.17
B
residues
isotrends
FTG 1, 2, 3, 4
143Nd/144Nd
147Sm/144Nd
0.5120
0.5115
0.5110
0.5105
0.5100
0.08
0.10
0.12
0.14
0.16

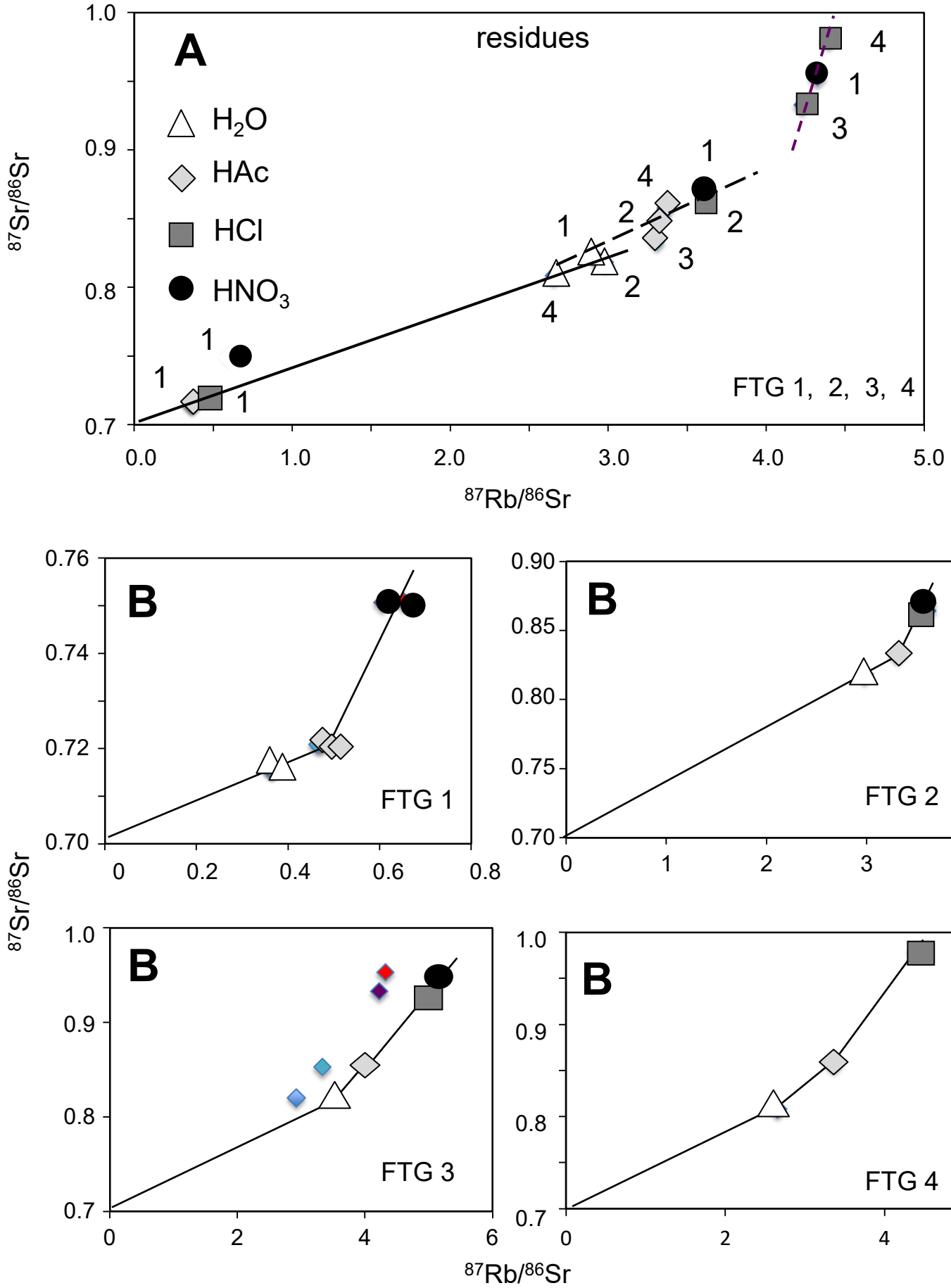
A
residues
H2O
HAc
HCl
HNO3
FTG 1, 2, 3, 4
87Sr/86Sr
87Rb/86Sr
B
FTG 1
FTG 2
FTG 3
FTG 4

| Sample IDs | removed by $H_2O$ (%) | left after $H_2O$ leaching (%) | removed by HAc (%) | left after HAc leaching (%) | removed by HCl (%) | left after HCl leaching (%) | removed by $HNO_3$ (%) | left after $HNO_3$ leaching (%) | total removed (%) |
|---|---|---|---|---|---|---|---|---|---|
| FTG1 | 0.25 | 99.78 | 28.74 | 71.04 | nd | nd | nd | nd | nd |
| FTG1a | 0.12 | 99.98 | 22.44 | 77.44 | 31.48 | 45.96 | 0.46 | 45.50 | 54.50 |
| FTG1b | 0.24 | 99.76 | 23.82 | 75.93 | 30.06 | 45.87 | 1.16 | 44.71 | 55.30 |
| FTG2 | 0.42 | 99.58 | 7.18 | 92.41 | 8.90 | 83.51 | 1.14 | 82.36 | 17.64 |
| FTG3 | 0.26 | 99.74 | 5.80 | 93.94 | 11.97 | 81.97 | 2.86 | 79.11 | 20.89 |
| FTG4 | 0.40 | 99.60 | 12.09 | 87.51 | 11.99 | 75.52 | 0.55 | 74.97 | 25.04 |

nd stands for not determined

| Sample IDs | Al/Si | Mg/Si | Ca/Si | Fe/Si | Mn/Si | P/Si | Si/Al | Mg/Al | Ca/Al | Fe/Al | Mn/Al | P/Al | Mg/Ca | Mg/Fe | Ca/Fe | Fe/Mn |
|---|---|---|---|---|---|---|---|---|---|---|---|---|---|---|---|---|
| FTG1 | | | | | | | | | | | | | | | | |
| $LH_2O$ | 0.98 | 21.2 | 18.3 | 0.13 | 0.02 | nd | 1.02 | 21.7 | 18.7 | 0.13 | 0.02 | nd | 1.16 | 168 | 145 | 6.54 |
| $LaH_2O$ | 0.33 | 12.7 | 13.2 | 0.04 | 0.03 | nd | 3.00 | 38.2 | 39.6 | 0.13 | 0.09 | nd | 0.96 | 292 | 303 | 1.45 |
| LaHAc | 1.50 | 25.0 | 48.9 | 13.0 | 1.74 | nd | 0.67 | 16.7 | 32.6 | 8.68 | 1.16 | nd | 0.51 | 1.92 | 3.75 | 7.48 |
| LaHCl | 1.49 | 28.9 | 50.4 | 16.3 | 1.76 | 0.12 | 0.67 | 19.4 | 33.9 | 10.9 | 1.18 | 0.08 | 0.57 | 1.78 | 3.10 | 9.22 |
| $LaHNO_3$ | 1.10 | 2.54 | 5.67 | 1.43 | 0.21 | nd | 0.91 | 2.31 | 5.17 | 1.31 | 0.19 | nd | 0.45 | 1.77 | 3.95 | 6.81 |
| $LbH_2O$ | 0.30 | 12.7 | 15.0 | 0.03 | 0.04 | nd | 3.31 | 42.0 | 49.7 | 0.11 | 0.13 | nd | 0.84 | 397 | 470 | 0.79 |
| FTG2 | | | | | | | | | | | | | | | | |
| $LH_2O$ | 0.21 | 2.06 | 5.64 | 0.01 | 0.01 | nd | 4.85 | 10.0 | 27.4 | 0.05 | 0.05 | nd | 0.37 | 200 | 547 | 1.00 |
| LHAc | 1.55 | 7.16 | 15.8 | 7.68 | 0.54 | nd | 0.65 | 4.62 | 10.2 | 4.96 | 0.35 | nd | 0.45 | 0.93 | 2.05 | 14.1 |
| LHCl | 1.70 | 6.76 | 14.5 | 7.53 | 0.38 | 0.52 | 0.59 | 3.99 | 8.56 | 4.44 | 0.23 | 0.31 | 0.47 | 0.90 | 1.93 | 19.6 |
| $LHNO_3$ | 4.22 | 3.46 | 5.30 | 9.45 | 0.17 | nd | 0.24 | 0.82 | 1.26 | 2.24 | 0.04 | nd | 0.65 | 0.37 | 0.56 | 55.4 |
| FTG3 | | | | | | | | | | | | | | | | |
| $LH_2O$ | 0.06 | 1.97 | 6.68 | 0.00 | 0.01 | nd | 16.0 | 31.5 | 107 | 0.08 | 0.12 | nd | 0.29 | 410 | 1390 | 0.67 |
| LHAc | 2.73 | 45.9 | 121 | 55.2 | 4.48 | nd | 0.37 | 16.8 | 44.4 | 20.2 | 1.64 | nd | 0.38 | 0.83 | 2.20 | 12.3 |
| LHCl | 1.31 | 32.7 | 75.6 | 39.4 | 2.29 | 0.85 | 0.76 | 24.9 | 57.6 | 30.0 | 1.74 | 0.65 | 0.43 | 0.83 | 1.92 | 17.2 |
| $LHNO_3$ | 0.84 | 16.0 | 37.2 | 19.1 | 1.35 | nd | 1.19 | 19.2 | 44.4 | 22.9 | 1.61 | nd | 0.43 | 0.84 | 1.94 | 14.2 |
| FTG4 | | | | | | | | | | | | | | | | |
| $LH_2O$ | 0.29 | 1.86 | 4.90 | 0.01 | 0.00 | nd | 3.42 | 6.35 | 16.7 | 0.03 | 0.01 | nd | 0.38 | 217 | 573 | 2.80 |
| LHAc | 2.18 | 11.0 | 26.7 | 13.8 | 0.92 | nd | 0.46 | 5.04 | 12.3 | 6.33 | 0.42 | nd | 0.41 | 0.80 | 1.94 | 15.0 |
| LHCl | 1.58 | 6.50 | 14.5 | 8.17 | 0.48 | 0.20 | 0.63 | 4.11 | 9.19 | 5.17 | 0.30 | 0.13 | 0.45 | 0.80 | 1.78 | 17.0 |
| $LHNO_3$ | 3.01 | 0.73 | 0.64 | 1.61 | 0.07 | nd | 0.33 | 0.24 | 0.21 | 0.53 | 0.02 | nd | 1.14 | 0.45 | 0.40 | 24.4 |

nd stands for not determined

| Sample IDs | ΣREE (μg/g) | Δ REE after leaching (μg/g) | Δ REE after leaching and before next step |
|---|---|---|---|
| FTG1 | | | |
| WR | 24.04 | | |
| HAc leachate | 25.04 | + 1.00 | + 1.00 |
| HAca leachate | 24.05 | + 0.10 | + 0.10 |
| HAcb leachate | 24.04 | 0 | 0 |
| HCl leachate | 19.00 | - 5.04 | - 5.04 |
| HClb leachate | 19.32 | - 4.72 | - 4.72 |
| $HNO_3$a leachate | 14.25 | - 9.79 | - 5.07 |
| $HNO_3$b leachate | 15.27 | - 8.79 | - 4.07 |
| | | | |
| FTG2 | | | |
| WR | 133.3 | | |
| HAc leachate | 133.2 | - 0.1 | - 0.1 |
| HCl leachate | 129.6 | - 3.70 | - 3.60 |
| $HNO_3$ leachate | 119.4 | - 13.9 | - 10.1 |
| | | | |
| FTG3 | | | |
| WR | 58.23 | | |
| HAc leachate | 58.25 | 0 | 0 |
| HCl leachate | 55.89 | - 2.34 | - 2.36 |
| $HNO_3$ leachate | 49.49 | - 8.74 | - 5.40 |
| | | | |
| FTG4 | | | |
| WR | 67.61 | | |
| HAc leachate | 67.61 | 0 | 0 |
| HCl leachate | 62.65 | - 4.94 | - 4.94 |
| $HNO_3$ leachate | 54.65 | - 12.96 | - 7.98 |

The successive leaching steps are $H_2O$, HAc, HCl and $HNO_3$,Σ □□□□□□ for□total amounts and Δ for the difference with previous step

| Sample IDs | La | Ce | Pr | Nd | Sm | Eu | Gd | Tb | Dy | Ho | Er | Tm | Yb | Lu | Σ REE |
|---|---|---|---|---|---|---|---|---|---|---|---|---|---|---|---|
| FTG1 | | | | | | | | | | | | | | | |
| WR | 4.62 | 8.43 | 0.94 | 4.04 | 1.10 | 0.79 | 1.30 | 0.19 | 1.05 | 0.24 | 0.62 | 0.11 | 0.52 | 0.09 | 24.04 |
| LHAc | 0.84 | 1.71 | 0.20 | 1.05 | 0.39 | 0.28 | 0.46 | 0.05 | 0.35 | 0.06 | 0.19 | 0.03 | 0.20 | 0.03 | 5.84 |
| RHAc | 3.78 | 6.72 | 0.74 | 2.99 | 0.71 | 0.51 | 0.84 | 1.14 | 0.70 | 0.18 | 0.43 | 0.08 | 0.32 | 0.06 | 19.20 |
| LaHAc | 0.73 | 1.52 | 0.18 | 0.87 | 0.30 | 0.24 | 0.36 | 0.05 | 0.31 | 0.06 | 0.19 | 0.03 | 0.18 | 0.04 | 5.06 |
| RaHAc | 3.89 | 6.91 | 0.76 | 3.17 | 0.80 | 0.55 | 0.94 | 0.14 | 0.74 | 0.19 | 0.43 | 0.08 | 0.34 | 0.05 | 18.99 |
| LbHAc | 0.68 | 1.40 | 0.17 | 0.84 | 0.30 | 0.24 | 0.34 | 0.05 | 0.28 | 0.05 | 0.15 | 0.03 | 0.16 | 0.03 | 4.72 |
| RbHAc | 3.94 | 7.03 | 0.77 | 3.20 | 0.80 | 0.55 | 0.96 | 0.14 | 0.77 | 0.19 | 0.47 | 0.08 | 0.36 | 0.06 | 19.32 |
| LaHCl | 0.66 | 1.44 | 0.17 | 0.85 | 0.29 | 0.14 | 0.37 | 0.05 | 0.34 | 0.06 | 0.19 | 0.02 | 0.16 | 0.02 | 4.76 |
| RaHCl | 3.23 | 5.47 | 0.59 | 2.33 | 0.51 | 0.41 | 0.57 | 0.09 | 0.40 | 0.13 | 0.24 | 0.06 | 0.18 | 0.03 | 14.24 |
| LbHCl | 0.59 | 1.24 | 0.15 | 0.73 | 0.21 | 0.13 | 0.29 | 0.04 | 0.30 | 0.05 | 0.16 | 0.02 | 0.13 | 0.03 | 4.07 |
| RbHCl | 3.35 | 5.79 | 0.62 | 2.47 | 0.59 | 0.42 | 0.67 | 0.10 | 0.47 | 0.14 | 0.31 | 0.06 | 0.23 | 0.03 | 15.25 |
| $LaHNO_3$ | 0.09 | 0.21 | 0.03 | 0.11 | 0.02 | 0.02 | 0.02 | 0.003 | 0.01 | 0.003 | 0.009 | 0.001 | 0.009 | 0.001 | 0.54 |
| $RaHNO_3$ | 3.15 | 5.26 | 0.56 | 2.22 | 0.48 | 0.39 | 0.55 | 0.09 | 0.39 | 0.13 | 0.23 | 0.06 | 0.17 | 0.03 | 13.71 |
| $LbHNO_3$ | 0.10 | 0.23 | 0.03 | 0.12 | 0.03 | 0.03 | 0.03 | 0.002 | 0.01 | 0.002 | 0.008 | 0.001 | 0.006 | 0.001 | 0.60 |
| $RbHNO_3$ | 3.25 | 5.56 | 0.59 | 2.36 | 0.57 | 0.39 | 0.65 | 0.10 | 0.46 | 0.13 | 0.30 | 0.06 | 0.22 | 0.03 | 14.67 |
| FTG2 | | | | | | | | | | | | | | | |
| WR | 28.53 | 55.22 | 6.56 | 24.52 | 4.36 | 3.03 | 4.76 | 0.52 | 2.54 | 0.47 | 1.38 | 0.15 | 1.06 | 0.17 | 133.3 |
| LHAc | 0.54 | 1.24 | 0.14 | 0.67 | 0.18 | 0.13 | 0.25 | 0.04 | 0.25 | 0.04 | 0.11 | 0.02 | 0.10 | 0.02 | 3.73 |
| RHAc | 27.99 | 53.98 | 6.42 | 23.85 | 4.18 | 2.90 | 4.51 | 0.48 | 2.29 | 0.43 | 1.27 | 0.13 | 0.96 | 0.15 | 129.5 |
| LHCl | 1.27 | 3.54 | 0.47 | 2.32 | 0.64 | 0.17 | 0.71 | 0.10 | 0.48 | 0.07 | 0.20 | 0.02 | 0.14 | 0.02 | 10.15 |
| RHCl | 26.72 | 50.44 | 5.95 | 21.53 | 3.54 | 2.73 | 3.80 | 0.38 | 1.82 | 0.37 | 1.07 | 0.11 | 0.81 | 0.13 | 119.4 |
| $LHNO_3$ | 0.35 | 0.83 | 0.09 | 0.39 | 0.06 | 0.03 | 0.06 | 0.005 | 0.03 | 0.004 | 0.01 | 0.002 | 0.008 | 0.002 | 1.871 |
| $RHNO_3$ | 26.37 | 49.60 | 5.85 | 21.14 | 3.48 | 2.70 | 3.74 | 0.38 | 1.79 | 0.36 | 1.06 | 0.11 | 0.81 | 0.13 | 117.5 |
| FTG3 | | | | | | | | | | | | | | | |
| WR | 11.53 | 23.06 | 2.75 | 10.50 | 2.19 | 1.26 | 2.42 | 0.30 | 1.84 | 0.34 | 0.95 | 0.08 | 0.88 | 0.13 | 58.23 |
| LHAc | 0.36 | 0.78 | 0.10 | 0.46 | 0.13 | 0.08 | 0.14 | 0.02 | 0.11 | 0.02 | 0.06 | 0.008 | 0.05 | 0.01 | 2.33 |
| RHAc | 11.17 | 22.28 | 2.65 | 10.04 | 2.06 | 1.19 | 2.28 | 0.28 | 1.73 | 0.32 | 0.89 | 0.08 | 0.83 | 0.12 | 55.92 |
| LHCl | 0.89 | 2.21 | 0.27 | 1.37 | 0.37 | 0.15 | 0.42 | 0.06 | 0.33 | 0.05 | 0.13 | 0.02 | 0.12 | 0.02 | 6.41 |
| RHCl | 10.28 | 20.07 | 2.38 | 8.67 | 1.69 | 1.03 | 1.85 | 0.22 | 1.39 | 0.27 | 0.76 | 0.06 | 0.71 | 0.10 | 49.48 |
| $LHNO_3$ | 0.38 | 0.91 | 0.10 | 0.43 | 0.09 | 0.03 | 0.09 | 0.01 | 0.06 | 0.009 | 0.03 | 0.004 | 0.02 | 0.003 | 2.17 |
| $RHNO_3$ | 9.90 | 19.16 | 2.28 | 8.24 | 1.60 | 1.00 | 1.76 | 0.21 | 1.34 | 0.26 | 0.73 | 0.05 | 0.69 | 0.10 | 47.32 |
| FTG4 | | | | | | | | | | | | | | | |
| WR | 13.93 | 26.85 | 3.15 | 12.18 | 2.50 | 1.40 | 2.39 | 0.33 | 1.81 | 0.43 | 1.13 | 0.14 | 1.21 | 0.16 | 67.61 |
| 0LHAc | 0.78 | 1.75 | 0.20 | 0.96 | 0.24 | 0.17 | 0.28 | 0.04 | 0.24 | 0.04 | 0.11 | 0.02 | 0.12 | 0.02 | 4.97 |
| RHAc | 13.15 | 25.10 | 2.95 | 11.22 | 2.26 | 1.23 | 2.11 | 0.29 | 1.57 | 0.39 | 1.02 | 0.12 | 1.09 | 0.14 | 62.64 |
| LHCl | 1.11 | 2.69 | 0.35 | 1.66 | 0.46 | 0.20 | 0.57 | 0.07 | 0.41 | 0.06 | 0.19 | 0.02 | 0.18 | 0.02 | 7.99 |
| RHCl | 12.05 | 22.40 | 2.60 | 9.57 | 1.81 | 1.03 | 1.54 | 0.21 | 1.16 | 0.33 | 0.83 | 0.10 | 0.91 | 0.12 | 54.66 |
| $LHNO_3$ | 0.34 | 0.71 | 0.08 | 0.31 | 0.05 | 0.02 | 0.04 | 0.004 | 0.02 | 0.003 | 0.01 | 0.001 | 0.005 | 0.001 | 1.59 |
| $RHNO_3$ | 11.71 | 21.69 | 2.52 | 9.26 | 1.76 | 1.01 | 1.49 | 0.21 | 1.14 | 0.32 | 0.82 | 0.10 | 0.91 | 0.12 | 53.06 |

Σ □□□□□□□□□□□□□□□□□

| Sample IDs | $^{87}Rb/^{86}Sr$ | Δ duplicates (± 2σ) | $^{87}Sr/^{86}Sr$ | $^{147}Sm/^{144}Nd$ | Δ duplicates (± 2σ) | $^{143}Nd/^{144}Nd$ |
|---|---|---|---|---|---|---|
| FTG1 | | | | | | |
| WR | 0.3691 | | 0.715911 | | | |
| $RH_2O$ | 0.3620 | | 0.715755 | 0.1541 | | 0.5114924 |
| $RaH_2O$ | 0.3656 | ± 0.5% | | | | |
| $RbH_2O$ | 0.3660 | ± 0.6% | | | | |
| LHAc | 0.0932 | | 0.709280 | | | |
| LaHAc | 0.0981 | ± 2.6% | | 0.2121 | | 0.5123555 |
| LbHAc | 0.1007 | ± 2.3% | | 0.2165 | ± 1.1% | |
| RHAc | 0.4935 | | 0.720857 | 0.1313 | | 0.5112473 |
| RaHAc | 0.4715 | ± 2.3% | | 0.1389 | ±2.9% | |
| RbHAc | 0.4630 | ± 3.1% | | 0.1384 | ± 2.7% | |
| LaHCl | 0.0362 | | 0.704651 | 0.2076 | | 0.5122928 |
| LbHCl | | | | 0.1733 | ± 8.3% | |
| $LaHNO_3$ | 0.5231 | | 0.711000 | 0.1257 | | 0.5115660 |
| $LbHNO_3$ | 0.6221 | ± 9.0% | | 0.1363 | ± 4.2% | |
| $RHNO_3$ | 0.6524 | | 0.750623 | 0.1146 | | 0.5110959 |
| $RaHNO_3$ | 0.6048 | ± 3.7% | | 0.1282 | ± 6.0% | |
| | | | | | | |
| FTG2 | | | | | | |
| WR | 2.9784 | | 0.818820 | | | |
| $RH_2O$ | 2.9776 | | 0.818141 | 0.1066 | | 0.5106722 |
| LHAc | 0.2482 | | 0.732237 | 0.1610 | | 0.5117447 |
| RHAc | 3.3071 | | 0.832956 | 0.1051 | | 0.5106597 |
| LHCl | 0.1748 | | 0.716810 | 0.1666 | | 0.5116317 |
| RHCl | 3.6048 | | 0.864351 | 0.0989 | | 0.5103987 |
| $LHNO_3$ | | | | 0.0912 | | 0.5109811 |
| $RHNO_3$ | 3.6072 | | 0.864967 | 0.0991 | | 0.5104668 |
| | | | | | | |
| FTG3 | | | | | | |
| WR | 2.9242 | | 0.816945 | | | |
| $RH_2O$ | 2.9334 | | 0.819994 | 0.1177 | | 0.5108943 |
| LHAc | 0.0428 | | 0.715848 | 0.1673 | | 0.5118425 |
| RHAc | 3.3344 | | 0.852722 | 0.1155 | | 0.5108468 |
| LHCl | 0.0261 | | 0.710414 | 0.1639 | | 0.5117936 |
| RHCl | 4.2271 | | 0.932831 | 0.1081 | | 0.5105603 |
| $LHNO_3$ | 0.2185 | | 0.713684 | 0.1222 | | 0.5112813 |
| $RHNO_3$ | 4.3224 | | 0.952914 | 0.1073 | | 0.5104942 |
| | | | | | | |
| FTG4 | | | | | | |
| WR | 2.6639 | | 0.808146 | | | |
| $RH_2O$ | 2.6536 | | 0.808361 | 0.1140 | | 0.5108097 |
| LHAc | 0.2202 | | 0.729089 | 0.1493 | | 0.5116862 |
| RHAc | 3.3605 | | 0.857557 | 0.1113 | | 0.5107080 |
| LHCl | 0.1415 | | 0.714659 | 0.1663 | | 0.5117872 |
| RHCl | 4.3939 | | 0.980399 | 0.1027 | | 0.5104699 |
| $LHNO_3$ | 4.3294 | | 0.732991 | 0.0983 | | 0.5110541 |
| $RHNO_3$ | | | | 0.1029 | | 0.5104538 |

| Sample IDs | $^{206}Pb/^{204}Pb$ | (±2σ) | $^{207}Pb/^{204}Pb$ | (±2σ) |
|---|---|---|---|---|
| FTG1 | | | | |
| $RH_2O$ | 48.099 | 0.015 | 23.542 | 0.011 |
| LHAc | 46.156 | 0.014 | 23.511 | 0.011 |
| RHAc | 49.891 | 0.007 | 24.288 | 0.003 |
| LHCl | 46.088 | 0.014 | 23.556 | 0.011 |
| $LHNO_3$ | 50.018 | 0.016 | 23.794 | 0.011 |
| $RHNO_3$ | 51.650 | 0.001 | 24.891 | 0.001 |
| | | | | |
| FTG2 | | | | |
| $RH_2O$ | 44.291 | 0.014 | 20.643 | 0.009 |
| LHAc | 41.128 | 0.013 | 20.776 | 0.009 |
| LHCl | 40.257 | 0.013 | 20.508 | 0.009 |
| $LHNO_3$ | 42.610 | 0.013 | 20.417 | 0.009 |
| | | | | |
| FTG3 | | | | |
| $RH_2O$ | 39.524 | 0.012 | 19.723 | 0.009 |
| LHAc | 32.513 | 0.010 | 19.032 | 0.009 |
| LHCl | 32.355 | 0.010 | 19.234 | 0.009 |
| $LHNO_3$ | 31.230 | 0.010 | 18.957 | 0.009 |
| | | | | |
| FTG4 | | | | |
| $RH_2O$ | 45.731 | 0.014 | 20.911 | 0.010 |
| LHAc | 33.460 | 0.010 | 19.408 | 0.009 |
| LHCl | 32.142 | 0.010 | 19.189 | 0.009 |
| $LHNO_3$ | 35.163 | 0.011 | 19.582 | 0.009 |
| $RHNO_3$ | 47.365 | 0.018 | 21.588 | 0.008 |

| Sample IDs | Rb-Sr (1) | Rb-Sr (2) | Sm-Nd (1) | Sm-Nd (2) | Pb-Pb (1) | Pb-Pb (2) |
|---|---|---|---|---|---|---|
| FTG 1 | **2182 +/- 47** | | 2002 +/- 140 | | | |
| FTG 2 | **2971 +/- 64** | **2222 +/- 41** | 2831 +/- 560 | | 2800 +/- 260 (leach) | |
| FTG 3 | **2461 +/- 51** | | 2930 +/- 290 | 3343 +/- 440 | 2850 +/- 760 (leach) | |
| FTG 4 | 2824 +/- 87 | | 3922 +/- 490 | 1444 +/- 180 | **2032 +/- 48** | 2749 +/- 490 (leach) |